



HAL
open science

Calretinin-expressing neurons in the basal forebrain specifically contact granule cells in the olfactory bulb and modulate odor learning

Vlad Stefan Constantinescu, Shani Folschweiller, Tiziano Siri, Mariana Alonso, Didier de Saint Jan, Armen Saghatelyan

► To cite this version:

Vlad Stefan Constantinescu, Shani Folschweiller, Tiziano Siri, Mariana Alonso, Didier de Saint Jan, et al. Calretinin-expressing neurons in the basal forebrain specifically contact granule cells in the olfactory bulb and modulate odor learning. *Journal of Neuroscience*, 2025, pp.e1867232024. 10.1523/jneurosci.1867-23.2024 . hal-04913457

HAL Id: hal-04913457

<https://hal.science/hal-04913457v1>

Submitted on 27 Jan 2025

HAL is a multi-disciplinary open access archive for the deposit and dissemination of scientific research documents, whether they are published or not. The documents may come from teaching and research institutions in France or abroad, or from public or private research centers.

L'archive ouverte pluridisciplinaire **HAL**, est destinée au dépôt et à la diffusion de documents scientifiques de niveau recherche, publiés ou non, émanant des établissements d'enseignement et de recherche français ou étrangers, des laboratoires publics ou privés.



Distributed under a Creative Commons Attribution 4.0 International License

Research Articles | Cellular/Molecular

Calretinin-expressing neurons in the basal forebrain specifically contact granule cells in the olfactory bulb and modulate odor learning

<https://doi.org/10.1523/JNEUROSCI.1867-23.2024>

Received: 2 October 2023

Revised: 13 December 2024

Accepted: 21 December 2024

Copyright © 2025 the authors

This Early Release article has been peer reviewed and accepted, but has not been through the composition and copyediting processes. The final version may differ slightly in style or formatting and will contain links to any extended data.

Alerts: Sign up at www.jneurosci.org/alerts to receive customized email alerts when the fully formatted version of this article is published.

1 **Calretinin-expressing neurons in the basal forebrain specifically contact granule**
2 **cells in the olfactory bulb and modulate odor learning**

3
4 Vlad Stefan Constantinescu^{1,2,3}, Shani Folschweiller⁴, Tiziano Siri^{1,2}, Mariana Alonso⁵,
5 Didier De Saint Jan^{4,*}, Armen Saghatelyan^{1,2,3*}
6

7 ¹Department of Cellular and Molecular Medicine, University of Ottawa, Ottawa, ON,
8 Canada, K1N 6N5

9 ²CERVO Brain Research Center, Quebec City, QC, Canada G1J 2G3

10 ³Université Laval, Quebec City, QC, Canada G1V 0A6

11 ⁴Institut des Neurosciences Cellulaires et Intégratives, Centre National de la Recherche
12 Scientifique, Unité Propre de Recherche 3212, Université de Strasbourg, 67084,
13 Strasbourg, France

14 ⁵Institut Pasteur, Université Paris Cité, Centre National de la Recherche Scientifique,
15 Unité Mixte de Recherche 3571, Perception and Action Unit, F-75015, Paris, France
16

17 ***Correspondence:** Didier De Saint Jan (desaintjan@inci-cnrs.unistra.fr) and Armen
18 Saghatelyan (asaghate@uottawa.ca)
19

20 **Running Title:** The role of the basal forebrain in odor processing
21

22 **Keywords:** olfactory bulb, granule cells, basal forebrain, horizontal diagonal band of
23 Broca, magnocellular preoptic nucleus, calretinin, interneurons, odor discrimination, odor
24 learning
25

26 Number of pages: 34

27 Number of figures: 7

28 Number of words: Abstract – 228; Introduction – 701; Discussion – 1691

29 **Abstract**

30 GABAergic neurons in basal forebrain (BF) nuclei project densely to all layers of the
31 mouse main olfactory bulb (OB), the first relay in odor information processing. However,
32 BF projection neurons are diverse and the contribution of each subtype to odor
33 information processing is not known. In the present study, we used retrograde and
34 anterograde tracing methods together with whole-brain light-sheet analyses, patch-clamp
35 recordings coupled with optogenetic and chemogenetic approaches during spontaneous
36 odor discrimination, and go/no-go odor discrimination/learning tests to characterize the
37 synaptic targets in the OB of BF calretinin-expressing (CR+) GABAergic cells and to
38 reveal their functional implications. We used mice of either sex to show that OB-projecting
39 CR+ neurons innervate the bulbar granule cell layer but not the glomerular layer.
40 Optogenetic stimulation of CR+ axonal projections in OB slices elicited monosynaptic
41 GABAergic currents in granule cells (GCs). Retrograde rabies virus-based transsynaptic
42 tracing experiments confirmed these synaptic connections and further suggested that
43 CR+ neurons provide the principal, if not the unique, BF input onto GCs. Chemogenetic
44 inhibition of CR+ neurons in the BF of male mice did not affect odor discrimination in
45 habituation/dishabituation tasks but led to impairment in odor learning during go/no-go
46 odor-associative tasks. Our results revealed a subtype-specific projection pattern in the
47 OB of a select population of BF neurons and suggested that distinct BF GABAergic
48 projections have distinct effects on odor information processing and learning.

49

50 **Significance statement**

51 The basal forebrain projects densely into the olfactory bulb and plays an important role in
52 odor processing. The basal forebrain contains neurochemically distinct cellular
53 populations but the contribution of each subtype to odor information processing is not
54 known. We identified predominant, if not unique, synaptic connections between neurons
55 in the basal forebrain that are characterized by the expression of calretinin (CR) and
56 granule cells in the olfactory bulb. The detailed morpho-functional characterization of
57 these connections based on anterograde, retrograde, and rabies-based transsynaptic
58 labeling, patch-clamp recordings, optogenetics, and behavioral analyses indicated that

59 these connections are GABAergic in nature and suggested that CR-expressing neurons
60 in the basal forebrain are involved in odor learning.

61

62 **Introduction**

63 The olfactory system is essential for the survival of many animal species. It provides vital
64 information about the surrounding world and influences social and sexual behaviors. In
65 mammals, odor information is conveyed by olfactory sensory neurons, which are
66 embedded in the olfactory epithelium, into the olfactory bulb (OB) where it is transmitted
67 to mitral and tufted (M/T) cells, the principal output neurons. Bulbar principal cells convey
68 the information to other brain regions such as the olfactory cortex, olfactory tubercle,
69 amygdala, entorhinal cortex, and elsewhere, with no thalamic relay (Davis, 2004). Odor
70 information processing in the OB is supported by a wide variety of interneurons,
71 principally granule cells (GCs) in deep layers, periglomerular cells (PGCs) in the
72 glomerular layer, and short-axon cells distributed in different layers. GCs are the most
73 abundant population in the OB and have a very specific morpho-functional identity
74 (Breton-Provencher & Saghatelyan, 2012). These axonless neurons mediate reciprocal
75 inhibition through reciprocal dendro-dendritic synapses with the lateral dendrites of M/T
76 cells (Isaacson & Strowbridge, 1998; Schoppa *et al*, 1998) and regulate fast neuronal
77 synchronization in the bulbar network and odor discrimination (Abraham *et al*, 2010; Dalal
78 & Haddad, 2022; Fukunaga *et al*, 2014; Lepousez & Lledo, 2013; Nunes & Kuner, 2015).
79 GCs in the OB are sub-divided into distinct subtypes based on their localization patterns
80 (Lemasson *et al.*, 2005) and molecular profiles (Malvaut & Saghatelyan, 2016). These
81 subtypes have distinct morpho-functional properties (Lemasson *et al*, 2005) and regulate
82 specific types of olfactory behavior (Hardy *et al*, 2018; Malvaut *et al*, 2017).

83 Information processing in the OB is regulated not only by local interneurons but also by
84 long-ranging excitatory, inhibitory, and neuromodulatory projections from other brain
85 regions. All bulbar layers are densely innervated by centrifugal inputs from the basal
86 forebrain (BF), particularly from two adjacent nuclei, the horizontal limb of the diagonal
87 band of Broca (HDB), and the magnocellular preoptic nucleus (MCPO) (Gracia-Llanes *et*
88 *al*, 2010; Niedworok *et al*, 2012; Zaborszky *et al*, 1986). Projections from the HDB/MCPO

89 are cholinergic and GABAergic and impinge onto most OB neuronal subtypes including
90 GCs and PGCs (Case *et al*, 2017; De Saint Jan, 2022; Hanson *et al*, 2020; Nunez-Parra
91 *et al*, 2013; Sanz Diez *et al*, 2019; Villar *et al*, 2021) as well as M/T cells (Zhou *et al*,
92 2023). Pharmacogenetic inhibition of the whole population of BF GABAergic neurons
93 impairs odor discrimination in spontaneous habituation/dishabituation tasks (Nunez-Parra
94 *et al.*, 2013). However, HDB/MCPO GABAergic neurons are diverse and the exact
95 topological organization of their projections in OB layers and their functional roles in odor
96 information processing are not well understood.

97 HDB/MCPO neuronal subtypes are distinguished by their molecular marker profiles,
98 morpho-functional properties, and projection patterns (Gritti *et al*, 2003; McKenna *et al*,
99 2021). Distinct HDB/MCPO GABAergic subtypes can be defined based on the expression
100 of Ca²⁺-binding proteins such as parvalbumin (PV), calbindin (CB), and calretinin (CR)
101 (Gritti *et al.*, 2003; McKenna *et al.*, 2021; Zaborszky *et al*, 2005) or by neuropeptides such
102 as somatostatin (SOM) (Anaclet *et al*, 2018; Freund & Gulyas, 1991). Release properties
103 and the impacts of HDB/MCPO GABAergic inputs on bulbar interneurons are diverse and
104 target-specific (De Saint Jan, 2022; Sanz Diez *et al.*, 2019), suggesting that select
105 subtypes of HDB/MCPO GABAergic neurons may innervate specific targets in the OB.
106 To shed more light on the function and topological organization of HDB/MCPO neurons
107 in the OB, we used anterograde and retrograde tracing approaches together with light-
108 sheet analyses of OB-projecting CR+ neurons in the whole brain, patch-clamp recordings
109 combined with optogenetics, behavioral tests, and pharmacogenetic approaches. We
110 identified three subtypes of GABAergic neurons in the HDB/MCPO that project to the OB.
111 Moreover, we found a specific projection pattern for CR-expressing HDB/MCPO neurons
112 that principally innervate the GCL of the main OB but not the glomerular layer. We
113 demonstrated that CR+ HDB/MCPO neurons make GABAergic synaptic connections with
114 GCs and that pharmacogenetic inactivation of OB-projecting CR+ neurons locally, in the
115 HDB/MCPO, alter odor learning in an operant-conditioning go/no-go odor
116 discrimination/learning task but not odor discrimination in a habituation/dishabituation
117 task. These results suggested that distinct neuronal subtypes in the HDB/MCPO
118 contribute in their own and specific way to odor information processing based on their
119 pattern of synaptic connections with OB interneurons.

122 **Materials and methods**

123 **Animals**

124 The experiments were performed using 2- to 4-month-old C57Bl/6 wild-type mice, CR-
125 EGFP mice (Caputi *et al*, 2009), and Calretinin-Cre mice (CR-Cre; B6(Cg)-
126 *Calb2^{tm1(cre)Zjh}/J*; RRID:IMSR_JAX:010774) of either sex. All animal experiments were
127 approved by the Université Laval and University of Ottawa animal care and protection
128 committees according to the guidelines of the Canadian Council on Animal Care (CCAC)
129 and by the French Ministry and local ethic committee for animal experimentation
130 (CREMEAS at the University of Strasbourg, and CETEA at the Institute Pasteur). One to
131 four mice per cage were kept on a 12-h light/dark cycle at a constant temperature (22°C)
132 with food and water *ad libitum*, except for the behavioral experiments, where the mice
133 were housed individually and were partially water-deprived.

134

135 **Stereotaxic injections**

136 The mice were anesthetized either with an intraperitoneal injection of a ketamine (100
137 mg/kg), acepromazine (3 mg/kg), and medetomidine (1 mg/kg) mix or with isoflurane (2-
138 2.5% isoflurane, 1 L/min of oxygen) and were placed in a stereotaxic apparatus. Lidocaine
139 (1 mg/kg) was subcutaneously injected over the skull 3-5 min before the surgery. The
140 animals were placed on a heating pad set at 37°C, and their corporal temperature was
141 continuously monitored with a rectal probe. Paw and ocular reflexes were periodically
142 checked during surgery to determine the depth of the anesthesia. After suturing the
143 incision, the mice received an intraperitoneal injection of Metacam 100 (meloxicam; 5-10
144 mg/kg) or caprofen (20 mg/kg) and were rehydrated with a 0.5-1 mL subcutaneous
145 injection of 0.9% NaCl. Antisedan (atipamezol; 0.4 mg/kg) was also injected
146 intraperitoneally in mice anesthetized with ketamine/acepromazine/medetomidine. The
147 mice were then placed under a heating lamp during the awakening phase.

148 Retrograde tracer injections in the OB were given to CR-GFP (n=4) and C57BL6 mice
149 (n=4) of either sex. The injection site was approximately in the center of the OB rostral to
150 the anterior venous sinus and lateral to the central scissure. A solution containing red
151 fluorescent latex microbeads (200 to 600 mL, RetroBeads™; Lumafluor) diluted to 25%

152 or 50% in 0.9% NaCl or AlexaFluor™ 555 cholera toxin subunit B conjugate (Invitrogen,
153 Thermo Fisher Scientific #C34776) was injected 200-500 µm deep from the dura using a
154 glass pipette. The mice were sacrificed 3 to 6 days post-injection.

155 For the whole-brain light-sheet analyses of OB-projecting CR+ cells, retrograde AAV viral
156 particles (pAAV-EF1a-double floxed-hChR2(H134R)-EYFP-WPRE-HGHp, #20298-
157 AAVrg, Addgene) were injected into the OB of CR-Cre male mice (n=5). Two injections
158 per OB to target the ventro-anterior and dorso-posterior regions were given at the
159 following coordinates (relative to bregma): for the ventro-anterior part of the OB, anterior-
160 posterior (AP) 5.5 mm, medio-lateral (ML) ±0.9 mm, and dorso-ventral (DV) 1.8 mm; for
161 the dorso-posterior part of the OB, AP 5.3 mm, ML ±0.5, and DV 0.9. Two weeks post-
162 injection, the animals were transcardially perfused with ice-cold PBS supplemented with
163 10 U/mL of heparin, followed by ice-cold 4% PFA. The brains were extracted and were
164 incubated in a 4% PFA solution at 4°C for 24 h with gentle shaking. The brains were then
165 washed twice in PBS and were stored in PBS containing 0.02% sodium azide prior to
166 shipping to LifeCanvas Technologies (Cambridge, USA) for clearing and light-sheet
167 imaging.

168 For the optogenetic and axonal tracing experiments, viruses were injected into the
169 HDB/MCPO of CR-Cre mice of either sex. Small holes were drilled at the following
170 coordinates (relative to the bregma): AP 0.2-0.6 mm, ML ±1.2-1.4 mm, and DV 5.2-5.5
171 mm) and 200-500 nL of either AAV9-EF1a-DIO-hChR2(H134R)-EYFP-WPRE-HGH
172 (University of Pennsylvania Viral Vector Core), AAV9-EF1a-double floxed-
173 hChR2(H134R)-EYFP-WPRE-HGHpA (Addgene #20298), or AAV5.EF1a.DIO.ChETA-
174 EYFP (Addgene #26968) were injected. The mice were sacrificed 2-4 weeks post-
175 injection.

176 For the retrograde rabies virus-based transsynaptic tracing, a retroviral construct was
177 injected into the rostral migratory stream (RMS) of neonatal mice pups at P6 (n=3) to label
178 GCs, as previously described (Grelat *et al*, 2018). Briefly, P6 male pups were
179 anesthetized with isoflurane (3.5%; 372 mL/min; Iso-Vet, Piramal Healthcare) and were
180 positioned in a stereotaxic frame using a homemade cast. Small craniotomies were drilled
181 above the injection sites with a needle, and bilateral viral injections (350 nL per site) were

182 made into the RMS at the following coordinates: AP 2.4 mm, ML \pm 0.6 mm, and DV 2.7
183 mm from the skull surface. The skin was closed with adhesive cyanoacrylate (Vetbond;
184 3M). The pups were returned to their mother after recovery (30-60 min) on a warm pad.
185 The retrovirus used in this study expresses DsRed, a fluorescent red marker, and the G
186 and TVA proteins necessary for a RABV vector secondary infection and propagation
187 (Retro-G-TVE-DsREd; 1.85×10^8 infectious particles/mL; 350 nL per site; produced by
188 VVGT-SFR Necker). Rabies viral vector expressing GFP (RABV-GFP; 3.5×10^8 ffu/mL;
189 250 nL per site; a gift from the University of Munich, Germany) was injected into the OB
190 at the following coordinates AP 4.8 mm, ML \pm 0.8 mm, and DV 1 and 1.5 mm from the
191 brain surface, 16 weeks after the retro-G-TVA-DsRed injections. The animals were
192 sacrificed 7 days after the RABV injections. Immunostaining was performed to ensure
193 that GFP and DsRed fluorescence could be visualized. For each mouse, the staining was
194 performed on 1 out of 3 sagittal brain sections from one hemisphere to verify the
195 specificity of the monosynaptic tracing. Only mice in which starter cells were exclusively
196 located in the granule cell layer were included in the analysis.

197

198 **Pharmacogenetic AAV construct injections in the HDB/MCPO and CNO** 199 **administration**

200 To study the role of BF CR⁺ interneurons using a go/no-go olfactory discrimination task,
201 we inactivated CR⁺ cells in the HDB/MCPO using the Designer Receptors Exclusively
202 Activated by Designer Drugs (DREADDs) pharmacogenetic approach. CR-Cre male mice
203 were anesthetized with isoflurane (2-2.5% isoflurane, 1 L/min of oxygen) and were placed
204 on the stereotaxic frame as described above. The Cre-dependent AAV 2/8 EF1 α -DIO-
205 hM4D(Gi)-mCherry or AAV 2/8 EF1 α -DIO-GFP viral vectors were bilaterally injected into
206 the HDB/MCPO of the CR-Cre mice at AP 0.6 mm, ML \pm 1.2 mm, and DV 5.2 mm (relative
207 to bregma). The mice were subjected to go/no-go olfactory discrimination/learning training
208 4 weeks after the injection.

209 To specifically inhibit OB-projecting CR⁺ neurons in the HDB/MCPO of a different cohort
210 of CR-Cre male mice (n=14), we injected retrograde Cre-dependent DREADDs (pAAVrg-
211 hSyn-DIO-hM4D(Gi)-mCherry, # 44362-AAVrg, Addgene) or control (pAAVrg-hSyn-DIO-

212 mCherry, #50459-AAVrg, Addgene) viral particles into the OB. Small craniotomies were
213 bilaterally drilled above the injection sites, and the viral injections (300 nL per site) were
214 made into the OB at the following coordinates (relative to the bregma): for the ventro-
215 anterior part of the OB, AP 5.5 mm, ML \pm 0.9 mm, and DV 1.8 mm; and for the dorso-
216 posterior part of the OB, AP 5.3 mm, ML \pm 0.5, and DV 0.9. During the same surgery, fluid
217 cannulas (Doric Lenses, Canada) were installed bilaterally above the HDB/MCPO at the
218 following coordinates: AP 0.4-0.6 mm, ML 1.4 mm, and DV 5.2 mm. After allowing for
219 viral expression and recovery of the animals for 4 weeks, the animals were then subjected
220 to behavioral training.

221 DREADDs receptors were activated either by an intraperitoneal injection of clozapine-N-
222 oxide (CNO, 2 mg/kg; Tocris, Cat# 4936) or by an intracerebral CNO injection just above
223 the HDB/MCPO through fluid cannulas (100 μ M; Tocris, Cat# 4936). For the behavioral
224 experiments, both the experimental and control groups of mice received either an
225 intraperitoneal injection of CNO every day, 25-30 min before starting the go/no-go task,
226 which lasted approximately 60 min for each animal, or an intracerebral CNO injection via
227 cannulas every day 5-10 min before starting the go/no-go task, which lasted
228 approximately 45 min for each animal. No CNO was given during the training.

229 To estimate the specificity of the viral targeting approach and the percentage of
230 DREADDs-infected CR+ cells in the entire CR+ HDB population, we estimated the
231 percentage of CR-immunolabeled cells among the DREADDs-infected cells (i.e., CR+
232 among the mCherry+ virally labeled cells) and calculated the percentage of DREADDs-
233 infected CR+ cells in the entire CR+ cell population in the HDB (i.e., mCherry+ virally
234 labeled cells among the CR+ immunolabeled cells in the HDB). To do so, confocal images
235 were taken, and the co-expression of markers was verified in several optical sections.

236

237 **Tissue preservation and clearing, immunolabeling, and imaging**

238 PFA-fixed samples were preserved using SHIELD reagents (LifeCanvas Technologies)
239 according to the manufacturer's instructions (Park *et al.*, 2018). Samples were delipidated
240 using LifeCanvas Technologies Clear+ delipidation reagents. Following delipidation, the

241 samples were labeled using eFLASH (Yun *et al.*, 2019) technology, which
242 integrates stochastic electro-transport (Kim *et al.*, 2015) and SWITCH (Murray *et al.*,
243 2015), using a SmartBatch+ (or SmartLabel) device (LifeCanvas Technologies). We used
244 primary goat polyclonal anti-GFP (EnCor Biotechnology RRID: AB_2737371, 10 µg/brain)
245 and secondary donkey anti-goat 488 (Jackson Immunoresearch, RRID: AB_2336933) to
246 boost the signal. Propidium iodide (ThermoFisher Scientific, P3566, 48 µL/brain) labeling
247 was also used to perform the registration and alignment of sections to the Allen Brain
248 Atlas. After immunolabeling, the samples were incubated in 50% EasyIndex (RI = 1.52,
249 LifeCanvas Technologies) overnight at 37°C followed by a 24-h incubation in 100%
250 EasyIndex for refractive index matching. After index matching, the samples were imaged
251 using a SmartSPIM axially-swept light sheet microscope using a 3.6x objective (0.2 NA)
252 (LifeCanvas Technologies).

253 Acquired images were registered in the Allen Brain Atlas (Allen Institute:
254 <https://portal.brain-map.org/>) using an automated process (alignment performed by
255 LifeCanvas Technologies). A propidium iodide channel for each brain was registered to
256 an average Syto16 atlas (generated by LifeCanvas Technologies using previously
257 registered samples). Registration was performed using successive rigid, affine, and b-
258 spline warping algorithms (SimpleElastix: <https://simpleelastix.github.io/>).

260 Automated cell detection was performed by LifeCanvas Technologies using a custom
261 convolutional neural network created with the Tensorflow python package (Google). The
262 cell detection was performed by two networks in sequence. First, a fully-convolutional
263 detection network (<https://arxiv.org/abs/1605.06211v1>) based on a U-Net architecture
264 (<https://arxiv.org/abs/1505.04597v1>) was used to find possible positive locations.
265 Second, a convolutional network using a ResNet architecture
266 (<https://arxiv.org/abs/1512.03385v1>) was used to classify each location as positive or
267 negative. Each cell location was projected onto the Allen Brain Atlas in order to count the
268 number of cells for each atlas-defined region using the previously calculated Atlas
269 Registration.

270

271 **Acute brain slice preparation**

272 For the electrophysiological recordings in the OB, the mice were deeply anesthetized
273 (ketamine/xylazine, 10 and 1 mg/mL, respectively, 0.1 mL per 10 g of body weight) 3-5
274 weeks after the stereotaxic injections and were transcardiacally perfused with modified
275 oxygenated artificial cerebro-spinal fluid (ACSF) containing the following (in mM): 210.3
276 sucrose, 3 KCl, 2 CaCl₂·2H₂O, 1.3 MgCl₂·6H₂O, 26 NaHCO₃, 1.25 NaH₂PO₄·H₂O, and 20
277 glucose. The OBs were then quickly removed, and 250- μ m-thick horizontal sections were
278 cut using a vibratome (Microm HM 650V; ThermoFisher Scientific). The sections were
279 placed in oxygenated ACSF containing the following (in mM): 125 NaCl, 3 KCl, 2
280 CaCl₂·2H₂O, 1.3 MgCl₂·6H₂O, 26 NaHCO₃, 1.25 NaH₂PO₄·H₂O, and 20 glucose.

281 For the electrophysiological recordings in the HDB/MCPO, the brains were removed, and
282 coronal sections were prepared in ice-cold oxygenated ACSF containing the following (in
283 mM): 83 NaCl, 26.2 NaHCO₃, 1 NaH₂PO₄, 2.5 KCl, 3.3 MgSO₄, 0.5 CaCl₂, 70 sucrose,
284 and 22 D-glucose (pH 7.3, osmolarity 300 mOsm/L). Horizontal slices (300 μ m) were cut
285 using a vibratome (HM 650V; Microm International GmbH, Germany) in the same
286 solution. The sections were incubated for 30-40 min at 34°C and were then stored at room
287 temperature in oxygenated ACSF containing the following (in mM): 125 NaCl, 25
288 NaHCO₃, 2.5 KCl, 1.25 NaH₂PO₄, 1 MgCl₂, 2 CaCl₂ and 25 D-glucose.

289

290 **Electrophysiological recordings**

291 Patch-clamp whole-cell recordings were performed in oxygenated ACSF superfused at
292 a rate of 2 mL/min at approximately 35°C. Neurons were examined by differential
293 interference contrast (DIC) using a Slicescope microscope (Scientifica, UK) coupled to a
294 camera (CoolSNAP EZ, Photometrics, USA). Cells were recorded using glass pipettes
295 (resistance 3-6 M Ω for neurons in the HDB/MCPO, 7-9 M Ω for GCs in the OB) filled with
296 an intracellular solution containing the following (in mM): 135 K-gluconate, 2 MgCl₂,
297 0.025 CaCl₂, 1 EGTA, 4 Na-ATP, 0.5 Na-GTP, 10 HEPES (all from Sigma Aldrich,
298 USA), and 1 mg/mL of neurobiotin (Vector Labs, UK) or biocytin (Sigma-Aldrich, B4261)
299 (pH 7.2, 290 mOsm). Atto 594 (Sigma Aldrich) or Alexa Fluor 594 (Life Technology) (5-
300 20 μ M) was added to the intra-pipette solution to visualize the recorded cell. Recordings

301 were performed with a Multiclamp 700B amplifier (Molecular Devices, USA) and
302 Axograph X acquisition software at an acquisition frequency of 20 kHz. Series
303 resistances (R_s), membrane resistances (R_m), and membrane capacitances (C_m) were
304 calculated by fitting an exponential curve to the relaxation phase of a current generated
305 by a potential jump (-10 mV/15 ms) in voltage-clamp mode. Series resistances did not
306 exceed 10% of the membrane resistances and were not compensated. Discharge
307 patterns were examined in the current-clamp mode by injecting currents of increasing
308 magnitude and a duration of 0.5-1 s. To assess the activation threshold of the voltage-
309 gated Na^+ current (I_{Na^+}) and its peak amplitude, we delivered depolarizing pulses
310 ranging from -100 to 30 mV in 10-mV increments. Sodium currents were isolated by
311 subtracting the traces obtained with and without the application of TTX (1 μM , Tocris).
312 For optogenetic experiments, blue light stimuli were delivered from a LED lamp
313 (wavelength 490 nm) through the 40x objective. Evoked IPSCs were isolated by the
314 bath application of 6-nitro-7-sulfamoylbenzo[f]quinoxaline-2,3-dione (NBQX) (50 μM ;
315 Tocris) and D-2-amino-5-phosphonopentanoic acid (D-AP5, 50 μM ; Tocris) to block
316 glutamatergic activity, while bicuculline methiodide (BMI) (50 μM ; Tocris), a GABA_A
317 receptor antagonist, was used to block GABAergic transmission. The latency of opto-
318 induced currents was measured by subtracting the time of the stimulus onset from the
319 onset of the recorded currents in the GCs. We also measured the jitter of
320 optogenetically induced currents that reflects variations in the latencies of currents in
321 response to repeated (20-s intervals) blue light pulses.

322 To reveal the morphology of the recorded cells, the patch pipette was slowly retracted
323 after the recording to avoid damaging the cell body. The sections were then fixed in 4%
324 PFA overnight, washed three times in PBS, and incubated in blocking buffer (0.5% Triton
325 X-100 and 4% skim milk diluted in PBS) at room temperature for 90 min. The sections
326 were then incubated for 2 h in VECTASTAIN[®] ABC-HPR (PK-4000 kit; Vector Labs) and,
327 after three washes in PBS, were stained with Streptavidin Alexa Fluor[™] 546 conjugate
328 (S11225; ThermoFisher) at room temperature for 90 min. DAPI was used to label nuclei.
329 The sections were mounted in fluorescence mounting medium (Dako) and were kept at
330 4°C before imaging using a confocal microscope (Olympus).

331

332 **Immunohistochemistry**

333 Adult mice were deeply anesthetized by an intraperitoneal injection of a mixture of
334 xylazine (20 mg/kg) and ketamine (100 mg/kg) and were intracardially perfused with PBS
335 or 0.9% NaCl followed by 4% PFA. The brains were removed and were kept in 4% PFA
336 overnight. Sections (50 μ m) were cut using a vibrating blade microtome (Leica VT 1000S).
337 The sections were blocked for 2 h in a PBS solution containing 4% BSA or 5% goat serum
338 and 0.3% Triton X-100. They were then incubated overnight at 4°C with the following
339 primary antibodies: goat anti-choline acetyl transferase (ChAT, 1/500; Merck Millipore,
340 Darmstadt, Germany; cat. no. AB144P, RRID:AB_2079751), mouse anti-somatostatin
341 (SOM; 1/500; Genetex, Irvine, USA; cat. no. GTX71935, RRID: AB_383280), mouse anti-
342 parvalbumin (PV; 1/1000; MilliporeSigma cat. no. P3088, RRID:AB_477329), rabbit anti-
343 calretinin (CR; 1/1000; Swant, Switzerland; cat. no. 7697, RRID:AB_2721226), mouse
344 anti-calbindin D28K (CB; 1/1000; MilliporeSigma cat. no. C9848, RRID:AB_476894),
345 rabbit anti-GFP (A-11122, 1/1000, 24 h; ThermoFisher Scientific), chicken anti-GFP
346 (GFP-1020, 1/1000, 24 h; Aves or Abcam), or rabbit anti-mCherry (5993-100, 1/1000; 24
347 h; Biovision). After three washes in PBS, the sections were incubated for 2 h at room
348 temperature with the corresponding secondary antibodies. They were then washed three
349 times with PBS and were mounted in Prolong Diamond Antifade Mountant (P36961;
350 ThermoFisher Scientific). Images were acquired using either a TCS SP5 II confocal
351 microscope (Leica), an FV-1000 confocal microscope (Olympus), an LSM880
352 AxioObserver Z1; confocal microscope (Zeiss), or a NanoZoomer (Hamamatsu).
353 Immunostained, EYFP-expressing and CR-expressing cells were manually counted using
354 the Fiji software Cell Counter plugin. For the rabies experiments, images were acquired
355 using an LSM980 confocal microscope (LCI Plan-Neofluor 25X/NA 0.8; Zeiss). GFP+ and
356 GFP+/CR+ double-positive cells were counted manually throughout the entire stack of
357 optical slices cells in the HDB/MCPO (1-3 stacks per slice; 4-6 slices per mouse).

358

359 **Go/no-go olfactory discrimination learning**

360 The DREADDs (AAV 2/8 EF1 α -DIO-hM4D(Gi)-mCherry or pAAVrg-hSyn-DIO-hM4D(Gi)-
361 mCherry) or control GFP (AAV 2/5 CAG-GFP or pAAVrg-hSyn-DIO-mCherry) viral vector-
362 injected mice were partially water-deprived until they reached 80 to 85% of their initial
363 body weight before starting the go/no-go training. Three-to-four days before beginning
364 the go/no-go training sessions, they were provided with 2 mL of water per day. This time
365 is usually sufficient for the mice to reach 80-85% of their body weight. They were weighed
366 twice every day and an additional amount of water was provided if the weight loss was
367 greater than 20%. After the start of the go/no-go training and test sessions, the animals
368 were still water-deprived and received water only during the training/test sessions through
369 the licking port (3 μ L/lick). At the end of the training/test day, the animals received a water
370 reward that did not exceed 1.5 mL of water through the same water port. After completion
371 of the go/no-go tests, the mice received water *ad libitum*. The animals were first trained
372 to insert their snouts into the odor sampling port and to lick the water port to receive a 3-
373 μ L water reward. The reward-associated odor (S+) was then introduced. The mice
374 initiated each trial by breaking the light beam across the odor sampling port, which opened
375 an odor valve. The duration of the opening was increased progressively from 0.1 to 1 s.
376 The main flowmeter was set at 1950 cc air/min, while the odor flowmeter, which carries
377 the flow from the odor vials to the water port, was set at 50 cc air/min. The mice with a
378 minimum sampling time of 50 ms received a water reward. They usually successfully
379 completed the training in one or two sessions. No differences between groups were
380 observed. All the mice went through one day of training/shaping. The animals had to lick
381 a water port through which they received the water reward when an odor was presented
382 to them. The time between the odor presentation and when the water reward was
383 delivered, was gradually increased from 0.1 s to 1.1 s. When the mice reached the 1.1-s
384 threshold and successfully licked 20 times, their training was considered complete. All the
385 animals spent approximately 40 min for the training/shaping session in one day. Following
386 the training procedure, the mice were subjected to the go/no-go odor discrimination task.
387 To ensure that they had successfully learned the task, the first session consisted of 30
388 trials during which only the S+ odor was presented. Mice that reached at least an 80%
389 success rate were then exposed randomly to a reward-associated odor (S+) or to a no
390 reward-associated odor (S-) for several blocks of 20 trials each (random exposure to 10

391 S+ and 10 S-). Correct responses consisted of correct hits (mouse licking the water port
392 after the S+ exposure) and correct rejections (mouse not licking the water port after the
393 S- exposure). False responses consisted of the mouse licking the water port after the S-
394 exposure or not licking the water port after the S+ exposure. The percentage of correct
395 responses for each block of 20 trials was calculated. The mice were considered to have
396 successfully completed the go/no-go olfactory discrimination task if they reached $\geq 85\%$
397 correct responses. The sessions lasted 2 to 6 days, depending on the odor pairs. The
398 following two odor pairs were used: odor pair 1, 0.1% octanal (S+ odor) vs. 0.1% decanal
399 (S- odor) in mineral oil and odor pair 2, 0.6% (+)-limonene + 0.4% (-)-limonene (S+ odor)
400 vs. 0.4% (+)-limonene + 0.6% (-)-limonene (S- odor) in mineral oil. The control and
401 experimental groups were both subjected to the same behavioral protocol with the same
402 exposure to the S+ and S- odors.

403

404 **Habituation/dishabituation odor discrimination task**

405 We performed an habituation/dishabituation spontaneous odor discrimination task with
406 CR-Cre male mice (n = 13 mice) that had been injected with Cre-dependent retrograde
407 AAV expressing either DREADDs (pAAVrg-hSyn-DIO-hM4D(Gi)-mCherry) or, as a
408 control, mCherry (pAAVrg-hSyn-DIO-mCherry) in the OB. The fluid cannulas for local
409 intracerebral delivery of CNO (100 μM) just above HDB/MCPO were installed in both
410 hemispheres during the same surgery. The stereotaxic injection and cannula installation
411 were performed as described above. The habituation/dishabituation odor discrimination
412 task was performed 4-5 weeks after viral injection. It consisted of three successive 4-min
413 trials with 6-min intervals between each exposure when the mice were presented with the
414 habituation odor (limonene(+), diluted 10^{-3}) followed by the dishabituation odor
415 (limonene(-), diluted 10^{-3}). During successive exposures to limonene(+), the total
416 investigation time progressively decreased as the mice became habituated to the odor.
417 The mice were considered to be able to discriminate the novel dishabituation odor
418 (limonene(-)) from the odor they were habituated to if the investigation time during the
419 dishabituation exposure was longer than the investigation time recorded during the third

420 and final habituation phases. CNO was injected into both groups of mice 5-10 min before
421 beginning the test.

422

423 **Statistics**

424 Data are expressed as means \pm SD unless otherwise indicated in the text. A Student's t-
425 test was used to assess the statistical difference between paired datasets with a normal
426 distribution, a non-parametric Wilcoxon-Mann-Whitney rank sum test to assess the
427 statistical difference between unpaired datasets, and a Kruskal-Wallis test for datasets
428 with more than two variables. The exact value of n and its representation (cells, animals)
429 are indicated in the text. No statistical methods were used to predetermine the sample
430 size. Equality of variance for the unpaired t-test was verified using the F-test. The levels
431 of significance were as follows: * $p < 0.05$, ** $p < 0.01$, and *** $p < 0.001$. When possible, the
432 investigator was blinded to the experimental conditions. Most of the experiments reported
433 herein were confirmed independently in two different labs, one at Université Laval and
434 the other at Université de Strasbourg.

435 Results

436 Multiple neuron subtypes in the HDB/MCPO project to the OB

437 To identify BF neurons that project to the OB, we first employed a retrograde tracing
438 approach (**Fig. 1A**) in which fluorescent microbeads (MB) (**Fig. 1B**) or Alexa Fluor
439 conjugates of the Cholera Toxin subunit B (CTB) (**Fig. 1C-D**) were injected into one OB.
440 Both tracers retrogradely labeled neuronal cell bodies in several regions of the brain, as
441 previously described (Hook & Puche, 2023; Santiago & Shammah-Lagnado, 2004;
442 Shipley & Adamek, 1984; Zaborszky *et al.*, 1986). Along a rostro-caudal axis, a high
443 density of MB+ or CTB+ neurons was found bilaterally in the anterior olfactory nucleus
444 and ipsilaterally in the piriform cortex in BF nuclei and in the nucleus of the lateral olfactory
445 tract (regions posterior to the nLOT were not examined). In the BF, retrogradely labeled
446 OB-projecting neurons were found along a ~1-mm-long antero-posterior axis, with the
447 highest density of labeled cells in the HDB/MCPO at the level of the crossing of the
448 anterior commissure (**Fig. 1B-C**).

449 The OB receives dense GABAergic and cholinergic axonal projections from the
450 HDB/MCPO. To characterize which subtypes of HDB/MCPO neurons project to the OB,
451 we performed immunolabeling for CR, CB, PV, and SOM to label four non-overlapping
452 cell populations (Gritti *et al.*, 2003; Yang *et al.*, 2017). These four generic markers
453 essentially label some of the BF GABAergic neurons (Yang *et al.*, 2017), but CR and CB
454 are also expressed in subpopulations of BF glutamatergic neurons (McKenna *et al.*,
455 2021). We also used choline acetyltransferase (ChAT) staining to label cholinergic
456 neurons. These experiments were done on brain sections from the CTB-injected mice.
457 CR-expressing neurons constituted the largest population of retrogradely labeled
458 HDB/MCPO neurons (19% of the CTB+ neurons, n=56 CR+ cells out of 294 CTB+
459 neurons, n=4 sections from 3 mice) (**Fig. 1C**). Eleven percent of CTB+ neurons were PV+
460 (n=42 PV+ neurons out of 383 CTB+ neurons, 7 sections from 3 mice) and 7% were
461 SOM+ (n=26 SOM+ neurons out of 362 CTB+ neurons, n=4 sections from 3 mice) (**Fig.**
462 **1D**). Very little co-labeling was observed in CB-expressing HDB/MCPO neurons, with only
463 2% of the OB-projecting CTB+ neurons labeled with CB (n=10 CB+ cells out of 469 CTB+
464 neurons, n=8 sections from 4 mice). Co-labeling of CTB with ChAT was found in 9% of

465 HDB/MCPO retrogradely labeled neurons (n=61 ChAT+ neurons out of 678 CTB+
466 neurons, 9 sections from 3 mice). These data indicated that at least three known sub-
467 populations of BF GABAergic neurons project to the OB, indicating that these projections
468 are quite diverse.

469 We then concentrated on studying a single OB-projecting BF sub-population, i.e., those
470 expressing CR. We first performed rabies virus-based monosynaptic tracing to determine
471 whether CR+ neurons in the HDB/MCPO establish direct synaptic inputs with GCs, the
472 most abundant cells in the OB. As the majority of GCs are born during the early postnatal
473 period (Hinds, 1968; Lemasson *et al.*, 2005; Mirich *et al.*, 2002), we injected the retro-
474 TVA-G-DsRED vector into the RMS on postnatal day 6 (P6) to infect neuroblasts
475 migrating to the OB. We injected a RABV virus into the GCL 120 days later to trace first-
476 order pre-synaptic partners of the previously labelled neuroblasts that differentiated into
477 GCs (**Fig. 2A**). With this protocol, GCs in the OB that had integrated both the G-TVA retro
478 and the RABV became the starter cells that allowed retrograde RABV propagation to their
479 presynaptic monosynaptic inputs located in different brain regions. This protocol made it
480 possible to specifically label GCs but not principal neurons or short-axon cells located in
481 the GCL or PGCs located in the glomerular layer (**Fig. 2B-C**). To assess brain regions
482 that are monosynaptically connected to GCs, we analyzed serial sagittal brain sections
483 and observed dense labelling in the HDB/MCPO (**Fig. 2D-E**). Next, we performed
484 immunolabeling for CR (**Fig. 2E**) and observed that the vast majority (86.3%; n=416 CR+
485 out of 482 GFP+ cells, 50 slices from 3 mice) of presynaptic partners of GCs in the
486 HDB/MCPO are CR+ (**Fig. 2F**). These data indicated that CR+ neurons in the
487 HDB/MCPO establish monosynaptic connections with GCs in the OB and are thus a
488 major neuronal subtype by which neuronal assemblies of BF may regulate the activity of
489 GCs.

490 We next investigated the localization and axonal pattern of CR+ cells that project to the
491 OB throughout the entire brain. To do so, we injected retrograde Cre-dependent AAVs
492 into the GCL of the OB of CR-Cre mice, followed by whole-brain clearing and light-sheet
493 imaging (**Fig. 3A**). We observed dense labeling of axons in the GCL of the OB together
494 with some labeled GCs (**Fig. 3B-C**). Interestingly, we also observed neuronal labeling in

495 several brain regions such as the entorhinal cortex (**Fig. 3D**), subiculum (**Fig. 3E**), piriform
496 cortex (**Fig. 3F-G**), and different cortical areas, including the gustatory, somatosensory,
497 and agranular insular cortices (**Fig. 3H**). In line with our previous results from retrograde
498 tracer labeling (**Fig. 1**) and monosynaptic rabies tracing (**Fig. 2**), we also observed dense
499 neuronal labeling in the HDB/MCPO (n=3 mice; **Fig. 3F, 3I**).

500

501 **Optogenetic stimulation of CR-expressing HDB/MCPO neurons elicit** 502 **monosynaptic inhibitory currents in the GCs of the OB**

503 The results of the viral tracing suggested that CR-expressing neurons are an important
504 sub-population of HDB/MCPO neurons projecting to the OB. We thus examined the
505 projection pattern and functional connectivity of HDB/MCPO CR+ neurons within the OB
506 using an optogenetic approach. We injected an AAV encoding a Cre-inducible ChR2–
507 EYFP fusion protein into the HDB/MCPO of CR-Cre mice (**Fig. 4A**). To validate the
508 specificity of the Cre-dependent recombination, we performed immunolabeling for CR
509 and observed that the majority of ChR2–EYFP-expressing cells in the HDB/MCPO are
510 also immunolabeled for CR ($80 \pm 6\%$, n = 221 cells from 3 mice; **Fig. 4B**). Next, we
511 characterized the functional properties of HDB/MCPO neurons that express ChR2–
512 EYFP by performing whole-cell patch-clamp recordings in acute coronal slices (**Fig.**
513 **4C**). All the cells tested (n=11 from 3 mice) responded to a blue light photo-stimulation
514 (1-300-ms duration), with a large inward current in the voltage-clamp configuration
515 (peak amplitude 695 ± 354 pA at $V_h = -75$ mV, 100-ms pulses). In the current-clamp
516 mode, photo-stimulations evoked an irregular train of action potentials (mean frequency
517 46.7 ± 9 Hz in response to 300-ms blue light pulses) (**Fig. 4D**) similar to the responses
518 evoked by the injection of a depolarizing current step (**Fig. 4E**). The capacitance and
519 membrane resistance of the recorded cells were, respectively, 14.6 ± 4.1 pF and $465 \pm$
520 190 MOhms (n=11 cells). CR+ cells had lower capacitance values than the general
521 population of retrogradely labeled neurons in the HDB (26 ± 7 pF, n=15 cells, $p < 0.001$,
522 Wilcoxon-Mann Whitney test), suggesting that CR+ neurons are in general smaller than
523 other OB-projecting HDB/MCPO neurons.

524 We next examined the projection pattern of HDB/MCPO CR+ neurons in OB sections
525 from fixed brain slices in which an AAV encoding a Cre-inducible ChR2–EYFP fusion
526 protein had been injected into the HDB/MCPO (n=3 CR-Cre mice). We observed EYFP-
527 labeled axons in the entire GCL. Occasionally, a few fibers crossed the mitral cell layer
528 and entered the external plexiform layer but rarely, if ever, penetrated into the glomerular
529 layer (n=13 sections from 3 mice, **Fig. 5A**). These results suggested that CR+ neurons in
530 the HDB/MCPO selectively target interneurons in the GCL of the OB.

531 To assess the synaptic properties of the connections made by ChR2-expressing CR+
532 HDB/MCPO neurons within the GCL, we used whole-cell voltage-clamp recordings from
533 GCs in acute OB sections (**Fig. 5B-D**). Stimulating CR+ ChR2-expressing BF axons with
534 brief (1-5 ms) flashes of blue light evoked outward synaptic currents in GCs voltage-
535 clamped at 0 mV (**Fig. 5C**). Photo-evoked currents exhibited fast onset latencies ($2.2 \pm$
536 0.78 ms) and little jitter (274 ± 170 μ s), which is consistent with monosynaptic
537 transmission. To selectively isolate the source of these currents, we first recorded GC
538 responses under baseline conditions and then, following the application of NBQX and D-
539 AP5, the AMPA and NMDA receptor antagonists, respectively. No changes in the
540 amplitude of photo-evoked currents were observed following the NBQX and D-AP5
541 applications (n=10 GCs from 7 mice; **Fig. 5C**). Light-induced currents were, however,
542 completely abolished by bicuculline methiodide (BMI), the GABA_A receptor antagonist
543 (n=10 GCs, **Fig. 5C**). These results are in line with the monosynaptic rabies viral tracing
544 and indicated that OB GCs receive monosynaptic GABAergic inputs from CR+ neurons
545 in the HDB/MCPO. Of the 32 GCs recorded in the GCL, 13 (40.6%) responded to the
546 photostimulation with an IPSC (n=7 mice). To assess whether GCs receiving synaptic
547 inputs from CR+ HDB/MCPO neurons are characterized by electrophysiologically distinct
548 properties compared to GCs that did not respond to the optogenetic stimulation, we
549 recorded passive and active membrane properties. No differences in the passive and
550 active membrane properties of responding and non-responding cells were observed (**Fig.**
551 **5D**). Overall, our results with viral tracing and electrophysiological analysis identified a
552 specific synaptic connection from CR+ neurons in the HDB/MCPO onto GCs in the OB.

553

554 **Pharmacogenetic inhibition of CR+ GABAergic neurons in the HDB/MCPO affect**
555 **olfactory discrimination and/or learning**

556 It has been previously shown that different subsets of GCs play distinct roles in odor
557 behavior (Hardy *et al.*, 2018; Malvaut *et al.*, 2017) and that HDB GABAergic projections
558 are involved in passive odor discrimination (Nunez-Parra *et al.*, 2013). However, the
559 HDB/MCPO GABAergic population is heterogeneous and it is not known how CR+ cells
560 are involved in odor discrimination and olfactory learning. To address this issue, we
561 employed a pharmacogenetic approach that specifically inhibits CR+ GABAergic neurons
562 in the HDB/MCPO and subjected the mice to the habituation/dishabituation odor
563 discrimination and go/no-go odor discrimination/learning tasks (**Fig. 6-7**). The Cre-
564 dependent AAVs expressing DREADDs coupled with mCherry were injected into the HDB
565 of the CR-Cre mice 4 weeks before beginning the behavioral task (**Fig. 6A-B**). We used
566 DREADDs coupled with a Gi protein. DREADDs-Gi activation by CNO leads to GIRK-
567 mediated K⁺ ion extrusion and hyperpolarization of the cell, which inhibits the activity of
568 these neurons. The control group of mice was injected with Cre-dependent AAV-GFP.
569 The two groups received a CNO injection 30 min prior to the task. Almost all the
570 DREADDs-infected cells were immunostained for CR ($95.8 \pm 0.9\%$), which made up 10.2
571 $\pm 0.7\%$ ($n = 996$ cells from 4 mice; **Fig. 6C**) of all HDB/MCPO CR+ GABAergic neurons.

572 We next subjected the mice to a go/no-go odor discrimination/learning task using different
573 odor combinations that progressively increased the difficulty of the task from a simple
574 odor pair (octanal vs. decanal, see Materials and Methods) to a more complex odor pair
575 [(0.6% (+)-limonene+0.4% (-)-limonene (S+ odor) vs. 0.4% (+)-limonene+0.6% (-)-
576 limonene (S- odor)] (**Fig. 6D-E**). As expected, the number of blocks needed to reach the
577 criterion of 85% correct responses increased with the difficulty of the discrimination task
578 for both the control and the DREADDs groups. Interestingly, inhibiting CR+ neurons in
579 the HDB/MCPO affected odor discrimination and/or learning in both the simple and the
580 complex tasks (**Fig. 6D-E**).

581 Although all the mice learned the task to criterion, the mean number of blocks required to
582 reach the 85% criterion was significantly higher for the DREADDs group than for the
583 control group when the mice were exposed to a simple task (the mean number of blocks

584 to reach the 85% criterion was 9 for the DREADDs group and 6 for the control group, n=7
585 and 5 mice, respectively, **Fig. 6D**). Statistically significant differences were also observed
586 in individual blocks beginning from block 5 to block 8 (**Fig. 6D**). The differences became
587 even more striking when the difficulty of the task was further increased with a complex
588 odor pair (**Fig. 6E**). The ability of the mice in the DREADDs group to discriminate the
589 odors was significantly lower than that of the mice in the control group (**Fig. 6E**). The
590 number of blocks needed to reach the 85% criterion was higher for the mice in the
591 DREADDs group. The mean number of blocks to reach the 85% criterion was 38 and 29
592 for the experimental and control groups, respectively (n=8 and 7 mice, respectively) (**Fig.**
593 **6E**). Significant differences in individual blocks were observed beginning from block 27
594 (**Fig. 6E**).

595 Although these results indicated that the HDB/MCPO CR+ neurons are involved in the
596 modulation of odor discrimination and/or learning in both the simple and complex go/no-
597 go tasks, the major drawback of these experiments is that the entire population of CR+
598 neurons in the BF is inhibited. It has been previously shown that HDB/MCPO neurons
599 innervate distinct cortical and subcortical brain areas to regulate arousal, motivation,
600 attention, learning, memory, and decision-making (Everitt & Robbins, 1997; Hanson *et al*,
601 2021; Klinkenberg *et al*, 2011; Lin *et al*, 2015; Nunez-Parra *et al*, 2020). It is thus possible
602 that the effects observed in the go/no-go odor discrimination/learning task following
603 systemic injection of CNO and the inhibition of the entire CR+ population in HDB/MCPO
604 is independent of the activity of GCs in the OB and is related to the changes in attention,
605 motivation, and/or reward-seeking behavior.

606 To address this caveat, we specifically inhibited OB-projecting CR+ cells in the
607 HDB/MCPO. To do so, we injected a retrograde Cre-dependent AAV expressing
608 DREADDs coupled with mCherry into the OB of CR-Cre mice. As a control, we used a
609 retrograde Cre-dependent AAV-mCherry. As the brain clearing and light-sheet analysis
610 had revealed several other brain regions in addition to HDB/MCPO that contain CR+ cells
611 projecting into the OB, we also installed fluid cannulas just above HDB/MCPO for the
612 local intracerebral delivery of CNO (100 μ M) in both groups of mice (**Fig. 6F**). This made
613 it possible to avoid inhibiting CR+ neurons in other brain areas. Both groups of mice

614 received comparable days and blocks of training with the go/no-go odor
615 discrimination/learning task and spent equal amounts of time to complete the training
616 (**Fig. 6G**). The viral injection resulted in specific labeling of CR+ cells in the HDB/MCPO
617 as $94.8 \pm 1.4\%$ of mCherry+ cells were also immunolabeled for CR (n=185 cells, **Fig. 6H**).
618 Importantly, intracerebral CNO infusion resulted in a significant decrease in
619 mCherry+/cfos+ cells in mice injected with DREADDs viral constructs, indicating that the
620 CNO infusion results in an effective inhibition of control and DREADDs-injected mice
621 ($35.2 \pm 1.1\%$ and $15.8 \pm 1.4\%$ for the control and DREADDs-injected mice, respectively;
622 n=339 and 537 mCherry+ cells analyzed, respectively, from 3 mice per group; **Fig. 6I-J**).
623 We next subjected the mice to a go/no-go odor discrimination/learning task using a simple
624 odor pair (octanal vs. decanal) followed by a more complex odor pair [(0.6% (+)-
625 carvone+0.4% (-)-carvone (S+ odor) vs. 0.4% (+)-carvone+0.6% (-)-carvone (S- odor)]
626 (**Fig. 6K-L**). Interestingly, inhibiting OB-projecting CR+ neurons in the HDB/MCPO
627 affected odor discrimination/learning only in the complex task but not in the simple go/no-
628 go task (**Fig. 6K-L**). The mean number of blocks required to reach the 85% criterion for
629 a simple go/no-go odor discrimination/learning task was comparable for both groups of
630 mice (n=6 and 8 for control and DREADDs-injected mice, respectively) (**Fig. 6K**). No
631 statistically significant differences were observed in individual blocks (**Fig. 6K**). In
632 contrast, statistically significant differences were observed in the complex go/no-go odor
633 discrimination/learning task (**Fig. 6L**). Pharmacogenetic inhibition of OB-projecting CR+
634 cells by intracerebral administration of CNO in the HDB/MCPO resulted in an increase in
635 the number of blocks needed to reach the 85% criterion (the mean number of blocks to
636 reach the 85% criterion was 22 and 32 for the control and experimental groups,
637 respectively, n=6 and 7 mice) (**Fig. 6L**), with significant differences in individual blocks
638 between both groups of mice (**Fig. 6L**).

639 These results suggested that local intracerebral inhibition of OB-projecting CR+ neurons
640 in the HDB/MCPO affects animal performance in the complex associative odor
641 discrimination/learning task. It remains, however, unclear whether these differences are
642 due to affected odor discrimination or learning. To address this issue, we subjected mice
643 to a passive habituation/dishabituation odor discrimination task (**Fig. 7**). In this task, both
644 groups of mice received an intracerebral injection of CNO (100 μ M) 5-10 min before

645 beginning the task and were exposed to the same odor (limonene(+)) using three
646 consecutive 4-min exposures with 6-min intervals between each exposure. The
647 investigation time during each consecutive exposure (habituation) decreased
648 progressively, indicating that the mice became habituated to the odor. For the final
649 presentation, the mice were presented with a novel odor (limonene(-)) alone for 4 min
650 and the investigation time was measured (**Fig. 7A**). Our results indicated that the
651 pharmacogenetic inhibition of OB-projecting CR+ neurons in the HDB/MCPO does not
652 affect the odor discrimination abilities of mice (**Fig. 7B**), suggesting that the differences
653 observed in the go/no-go odor associative task are due to affected odor learning abilities,
654 rather than odor discrimination.

655 Overall, our viral tracing, electrophysiological, and behavioral data indicated that long-
656 ranging CR+ cells in the HDB/MCPO establish monosynaptic GABAergic connections
657 with GCs in the OB and are required for learning complex odor mixtures.

658

659 **Discussion**

660 Local and long-ranging inhibitory circuits in the OB play an essential role in bulbar network
661 functioning and olfactory behavior. Odor information processing in the OB is under the
662 control of local interneurons such as PGCs and GCs that regulate the theta and gamma
663 rhythms in the bulbar network, respectively (Fukunaga *et al.*, 2014; Villar *et al.*, 2021).
664 Each of these two classes of local interneurons can be further subdivided into
665 heterogeneous cell populations based on their morpho-functional and molecular
666 properties that modulate different types of olfactory behavior in different ways (Hardy *et al.*,
667 2018; Malvaut *et al.*, 2017; Malvaut & Saghatelian, 2016). A growing body of evidence
668 has also revealed that long-ranging inhibitory projections, especially the GABAergic
669 inputs from the BF to OB neurons, play a role in bulbar network functioning and odor
670 processing (Bohm *et al.*, 2020; Nunez-Parra *et al.*, 2013; Sanz Diez *et al.*, 2019). However,
671 although the diversity of GABAergic neurons in the basal forebrain and, specifically in the
672 HDB/MCPO, is largely recognized (Freund & Gulyas, 1991; Gracia-Llanes *et al.*, 2010;
673 Gritti *et al.*, 2003; Hook & Puche, 2023; McKenna *et al.*, 2013; Niedworok *et al.*, 2012;
674 Nunez-Parra *et al.*, 2013; Sanz Diez *et al.*, 2019; Yang *et al.*, 2017; Zaborszky *et al.*,

675 2005), the contribution of specific inhibitory neuron subtypes in these regions is unknown.
676 In the present study, we identified specific HDB/MCPO GABAergic projections defined by
677 the expression of CR that are synaptically wired to GCs in the GCL of the main OB.
678 Optogenetic activation of HDB-derived CR+ axons in the OB elicited monosynaptic
679 GABAergic currents in GCs, while chemogenetic inactivation of the CR+ neurons in the
680 HDB/MCPO during spontaneous habituation/dishabituation odor discrimination and
681 go/no-go odor discrimination/learning tasks revealed an impairment in odor learning, but
682 not odor discrimination. Our results revealed that a particular cellular type in the
683 HDB/MCPO makes a specific contribution but, together with previous findings (Bohm *et*
684 *al.*, 2020; Nunez-Parra *et al.*, 2013; Sanz Diez *et al.*, 2019), also indicated that
685 HDB/MCPO GABAergic projections into the OB may have multiple and distinct
686 involvements in odor information processing and olfactory behavior.

687 Our morphometric retrograde and anterograde tracing results showed that there is a cell-
688 type-specific innervation of a subpopulation of GCs in the GCL by CR+ axons projecting
689 from the HDB/MCPO. This contrasts with the labeling pattern observed after targeting all
690 GABAergic neurons in the HDB/MCPO that results in the dense innervation of all bulbar
691 layers (Gracia-Llanes *et al.*, 2010; Hook & Puche, 2023; Niedworok *et al.*, 2012; Nunez-
692 Parra *et al.*, 2013; Sanz Diez *et al.*, 2019). The HDB/MCPO also contains a large
693 population of cholinergic neurons that mostly target the glomerular layer and the internal
694 plexiform layer (IPL) of the OB (Case *et al.*, 2017; De Saint Jan, 2022; Hamamoto *et al.*,
695 2017; Salcedo *et al.*, 2011). Recently, it has also been shown that HDB/MCPO cholinergic
696 and GABAergic projections contact different subtypes of PGCs and regulate their activity
697 in distinct ways (De Saint Jan, 2022). These results indicated that different bulbar
698 sublayers and OB cell subtypes are targeted by distinct HDB/MCPO neuronal subtypes
699 based on their molecular identities.

700 Interestingly, not all GCs in the GCL were synaptically connected to CR+ cells in the
701 HDB/MCPO. Our combined optogenetic stimulations of CR+ axons and
702 electrophysiological recordings from GCs showed that about 40% of these cells receive
703 a monosynaptic GABAergic input from CR+ cells in the HDB/MCPO. This is in part due
704 to an inherent technical limitation of our local injections, with viruses likely infecting only

705 a fraction of the OB-projecting CR+ neurons in the HDB/MCPO. These BF nuclei extend
706 for more than 1 mm on the rostro-caudal axis along which CR+ neurons are
707 heterogeneously distributed, making it difficult to infect the entire population (Zaborszky *et*
708 *al.*, 2005). However, we cannot exclude the possibility that HDB/MCPO CR+ neurons
709 target specific GC subtypes in the OB. GCs in the GCL are indeed heterogeneous and
710 can be distinguished based on their morphology (Merkle *et al.*, 2014) or by the expression
711 of molecular markers such as 5T4, CR, or CaMKII α (Hardy *et al.*, 2018; Malvaut *et al.*,
712 2017; Murata *et al.*, 2011). In the present study, we did not distinguish between the
713 molecular phenotypes of OB target cells during recording sessions, and it is unclear
714 whether GCs receiving cell-type specific connections from CR+ neurons in the
715 HDB/MCPO are distinct in terms of their molecular make-up or not. It is also conceivable
716 that CR+ HDB neurons contact early-born and adult-born GCs differently. We did not
717 distinguish between these subtypes, which have different synaptic (Lemasson *et al.*,
718 2005; Valley *et al.*, 2013) and intrinsic membrane (Belluzzi *et al.*, 2003; Carleton *et al.*,
719 2003) properties and play distinct roles in odor behavior (Alonso *et al.*, 2012; Breton-
720 Provencher *et al.*, 2009; Magavi *et al.*, 2005).

721 How do CR+ cells in the HDB affect olfactory behavior? To address this issue, we used
722 a pharmacogenetic approach and olfactory behavioral tests. We first used a go/no-go
723 operant-conditioning odor discrimination/learning paradigm in which the animals had to
724 discriminate between two distinct (simple task) or similar (difficult task) odors to receive a
725 water reward. The mice in which the activity of all CR+ cells in the HDB/MCPO was
726 inhibited through systemic injections of CNO displayed reduced odor
727 discriminatory/learning capabilities in both the simple and the complex odor tasks. The
728 reduced odor discrimination/learning in a simple task when the animals needed to
729 distinguish two very different odors was, however, intriguing. One clue may come from
730 the fact that HDB/MCPO neurons innervate distinct cortical and subcortical brain areas
731 to regulate arousal, attention, learning, memory, and decision-making (Everitt & Robbins,
732 1997; Hanson *et al.*, 2021; Klinkenberg *et al.*, 2011; Lin *et al.*, 2015; Nunez-Parra *et al.*,
733 2020). Both GABAergic and cholinergic neurons in the BF are recruited during go/no-go
734 odor discrimination tasks (Hanson *et al.*, 2021; Nunez-Parra *et al.*, 2020) and play a role
735 in sustaining attention (Hangya *et al.*, 2015) or encoding reward and motivational

736 information (Avila & Lin, 2014; Hanson *et al.*, 2021; Nguyen & Lin, 2014). Interestingly,
737 their responses are bi-phasic and increase during reward seeking behavior and decrease
738 with reward delivery in a go/no-go odor discrimination task (Hanson *et al.*, 2021). It is thus
739 conceivable that the role of HDB/MCPO CR+ cells in the go/no-go odor
740 discrimination/learning task goes beyond the modulation of bulbar network activity
741 through inhibitory contacts with GCs and may be due to their role in attention and reward-
742 seeking behavior through their connections with non-olfactory areas. To reveal the role
743 of OB-projecting CR+ neurons in the HDB/MCPO, we labeled these cells with retrograde
744 viral injections in the OB and inhibited their activity with the local intracerebral infusion of
745 CNO through fluid cannulas installed in the HDB/MCPO. Interestingly, inhibiting OB-
746 projecting CR+ neurons in the HDB/MCPO affected the complex but not the simple odor
747 discrimination/learning task. These data revealed, on the one hand, that CR+ neurons in
748 the HDB/MCPO make a specific contribution to modulating the odor
749 discrimination/learning of complex odor mixtures through their monosynaptic contacts
750 with OB GCs and, on the other hand, that other subtypes of CR+ neurons in the
751 HDB/MCPO may also affect the attention, reward-seeking, and motivation of mice
752 through their connections with the cortical and subcortical areas. This may influence
753 behavioral outcomes in both simple and complex go/no-go odor discrimination/learning
754 tasks when the entire population of CR+ cells in HDB/MCPO is inhibited. The reduction
755 in odor discrimination/learning following the local intracerebral inhibition of OB-projecting
756 CR+ cells in the HDB/MCPO was likely because the learning abilities of mice are affected
757 given that the pharmacogenetic inhibition of these cells did not affect odor discrimination
758 in the habituation/dishabituation task. Interestingly, previous studies have shown that the
759 pharmacogenetic inhibition of the entire GABAergic population of HDB/MCPO affected
760 odor discrimination in the spontaneous habituation/dishabituation task (Nunez-Parra *et*
761 *al.*, 2020; Nunez-Parra *et al.*, 2013). As the projection patterns of CR+ and other
762 GABAergic neurons of HDB/MCPO into OB are markedly different, and target exclusively
763 the GCL or the entire bulbar layer, respectively, these data suggested that the modulation
764 of the activity of these populations of cells may result in distinct behavioral outcomes.

765 The specific involvement of OB-projecting CR+ neurons in the HDB/MCPO in the odor
766 learning, but not habituation/dishabituation odor discrimination, is interesting as previous

767 studies have shown that inhibiting different subtypes or numbers of bulbar interneurons
768 affects complex odor discrimination/learning (Alonso *et al.*, 2012; Hardy *et al.*, 2018;
769 Lepousez & Lledo, 2013; Malvaut *et al.*, 2017), while optogenetic activation of GCs
770 improves complex task learning (Alonso *et al.*, 2012; Gschwend *et al.*, 2015) and odor-
771 reward association (Grelat *et al.*, 2018). It should be noted that, in all these experiments,
772 the pharmacogenetic, optogenetic, or pharmacological manipulation of GCs occurred in
773 the OB. In contrast, in the present study, we inhibited the activity of a select subtype of
774 GABAergic neurons in the HDB/MCPO, which should in turn disinhibit the activity of GCs.
775 How can an increase in the inhibition or disinhibition of GCs lead to the same behavioral
776 outcome? One clue may come from the subtype of GCs that receive selective inhibitory
777 inputs from CR+ cells in the HDB/MCPO. Depending on the molecular phenotype or
778 morpho-functional properties, different GC subtypes may play distinct roles in principal
779 cell activity in the OB (Malvaut & Saghatelian, 2016; Merkle *et al.*, 2014). For example,
780 several new subtypes of GCs in the superficial GCL have been described and, depending
781 on the location of their synaptic outputs, either in the somatic or dendritic domains of
782 principal cells, it has been proposed that they can affect odor information processing in
783 different ways (Merkle *et al.*, 2014). Our results provided additional evidence and point to
784 a major involvement of specific cell types in the HDB/MCPO defined by the expression of
785 CR in odor learning. This also warrants an investigation of the subtypes of OB GCs that
786 receive this specific synaptic input from CR+ cells in the BF as well as the roles of other
787 HDB/MCPO interneurons in olfactory behavior.

788 In conclusion, our experimental results showed that HDB/MCPO GABAergic projections
789 can have multiple and complex involvements in odor information processing and that the
790 HDB/MCPO projections defined by CR expression provide selective inhibitory inputs to
791 GCs in the OB and strongly influence odor learning.

792

793 **Acknowledgments**

794 This work was supported by a Canadian Institute of Health Research (CIHR) grant to A.S.
795 and by a Centre National de la Recherche Scientifique (CNRS) grant to D.D.S-J., We are

796 grateful to Dr. Karl-Klaus Conzelmann and Alexandru Adrian Hennrich (Max Von
797 Pettenkofer Institute Virology and Gene Center, Medical Faculty, Ludwig-Maximilians-
798 University Munich, Germany) for the generous gift of the (EnvA)SAD- Δ G-mCherry virus
799 and Dr. Benedikt Bennigner (University Medical Center of the Johannes Gutenberg
800 University, Mainz, Germany) for the retro-TVA-G plasmid construction. We thank the Cell
801 Biology and Image Acquisition (CBIA) Core Facility (RRID:SCR_021845) at the University
802 of Ottawa for the use of the various imaging systems and the Viral Vector for Gene
803 Transfer core facility of the Structure Fédérative de Recherche Necker for the retroviral
804 vector production. We also thank Aurelia Ces and Pierre Hener (ComptOpt platform and
805 morpho-functional analysis platform, respectively, Institut des Neurosciences Cellulaires
806 et Intégratives, Strasbourg) for their technical support.

807

808 **Declaration of interests**

809 The authors declare no competing interests.

810

811

812

813 **References**

814

- 815 Abraham NM, Egger V, Shimshek DR, Renden R, Fukunaga I, Sprengel R, Seeburg PH,
816 Klugmann M, Margrie TW, Schaefer AT *et al* (2010) Synaptic inhibition in the olfactory
817 bulb accelerates odor discrimination in mice. *Neuron* 65: 399-411
- 818 Alonso M, Lepousez G, Sebastien W, Bardy C, Gabellec MM, Torquet N, Lledo PM (2012)
819 Activation of adult-born neurons facilitates learning and memory. *Nat Neurosci* 15: 897-
820 904
- 821 Anaclet C, De Luca R, Venner A, Malyshevskaya O, Lazarus M, Arrigoni E, Fuller PM
822 (2018) Genetic Activation, Inactivation, and Deletion Reveal a Limited And Nuanced Role
823 for Somatostatin-Containing Basal Forebrain Neurons in Behavioral State Control. *J*
824 *Neurosci* 38: 5168-5181
- 825 Avila I, Lin SC (2014) Motivational salience signal in the basal forebrain is coupled with
826 faster and more precise decision speed. *PLoS Biol* 12: e1001811
- 827 Belluzzi O, Benedusi M, Ackman J, LoTurco JJ (2003) Electrophysiological differentiation
828 of new neurons in the olfactory bulb. *J Neurosci* 23: 10411-10418
- 829 Bohm E, Brunert D, Rothermel M (2020) Input dependent modulation of olfactory bulb
830 activity by HDB GABAergic projections. *Sci Rep* 10: 10696
- 831 Breton-Provencher V, Lemasson M, Peralta MR, 3rd, Saghatelian A (2009) Interneurons
832 produced in adulthood are required for the normal functioning of the olfactory bulb
833 network and for the execution of selected olfactory behaviors. *J Neurosci* 29: 15245-
834 15257
- 835 Breton-Provencher V, Saghatelian A (2012) Newborn neurons in the adult olfactory bulb:
836 unique properties for specific odor behavior. *Behav Brain Res* 227: 480-489
- 837 Caputi A, Rozov A, Blatow M, Monyer H (2009) Two calretinin-positive GABAergic cell
838 types in layer 2/3 of the mouse neocortex provide different forms of inhibition. *Cereb*
839 *Cortex* 19: 1345-1359
- 840 Carleton A, Petreanu LT, Lansford R, Alvarez-Buylla A, Lledo PM (2003) Becoming a new
841 neuron in the adult olfactory bulb. *Nat Neurosci* 6: 507-518
- 842 Case DT, Burton SD, Gedeon JY, Williams SG, Urban NN, Seal RP (2017) Layer- and
843 cell type-selective co-transmission by a basal forebrain cholinergic projection to the
844 olfactory bulb. *Nat Commun* 8: 652
- 845 Dalal T, Haddad R (2022) Upstream gamma-synchronization enhances odor processing
846 in downstream neurons. *Cell Rep* 39: 110693
- 847 Davis RL (2004) Olfactory learning. *Neuron* 44: 31-48
- 848 De Saint Jan D (2022) Target-specific control of olfactory bulb periglomerular cells by
849 GABAergic and cholinergic basal forebrain inputs. *Elife* 11

850 Everitt BJ, Robbins TW (1997) Central cholinergic systems and cognition. *Annu Rev*
851 *Psychol* 48: 649-684

852 Freund TF, Gulyas AI (1991) GABAergic interneurons containing calbindin D28K or
853 somatostatin are major targets of GABAergic basal forebrain afferents in the rat
854 neocortex. *J Comp Neurol* 314: 187-199

855 Fukunaga I, Herb JT, Kollo M, Boyden ES, Schaefer AT (2014) Independent control of
856 gamma and theta activity by distinct interneuron networks in the olfactory bulb. *Nat*
857 *Neurosci* 17: 1208-1216

858 Gracia-Llanes FJ, Crespo C, Blasco-Ibanez JM, Nacher J, Varea E, Rovira-Esteban L,
859 Martinez-Guijarro FJ (2010) GABAergic basal forebrain afferents innervate selectively
860 GABAergic targets in the main olfactory bulb. *Neuroscience* 170: 913-922

861 Grelat A, Benoit L, Wagner S, Moigneu C, Lledo PM, Alonso M (2018) Adult-born neurons
862 boost odor-reward association. *Proc Natl Acad Sci U S A* 115: 2514-2519

863 Gritti I, Manns ID, Mainville L, Jones BE (2003) Parvalbumin, calbindin, or calretinin in
864 cortically projecting and GABAergic, cholinergic, or glutamatergic basal forebrain neurons
865 of the rat. *J Comp Neurol* 458: 11-31

866 Gschwend O, Abraham NM, Lagier S, Begnaud F, Rodriguez I, Carleton A (2015)
867 Neuronal pattern separation in the olfactory bulb improves odor discrimination learning.
868 *Nat Neurosci* 18: 1474-1482

869 Hamamoto M, Kiyokage E, Sohn J, Hioki H, Harada T, Toida K (2017) Structural basis
870 for cholinergic regulation of neural circuits in the mouse olfactory bulb. *J Comp Neurol*
871 525: 574-591

872 Hangya B, Ranade SP, Lorenc M, Kepecs A (2015) Central Cholinergic Neurons Are
873 Rapidly Recruited by Reinforcement Feedback. *Cell* 162: 1155-1168

874 Hanson E, Brandel-Ankrapp KL, Arenkiel BR (2021) Dynamic Cholinergic Tone in the
875 Basal Forebrain Reflects Reward-Seeking and Reinforcement During Olfactory Behavior.
876 *Front Cell Neurosci* 15: 635837

877 Hanson E, Swanson J, Arenkiel BR (2020) GABAergic Input From the Basal Forebrain
878 Promotes the Survival of Adult-Born Neurons in the Mouse Olfactory Bulb. *Front Neural*
879 *Circuits* 14: 17

880 Hardy D, Malvaut S, Breton-Provencher V, Saghatelian A (2018) The role of calretinin-
881 expressing granule cells in olfactory bulb functions and odor behavior. *Sci Rep* 8: 9385

882 Hinds JW (1968) Autoradiographic study of histogenesis in the mouse olfactory bulb. I.
883 Time of origin of neurons and neuroglia. *J Comp Neurol* 134: 287-304

884 Hook C, Puche AC (2023) Bulbar projecting subcortical GABAergic neurons send
885 collateral branches extensively and selectively to primary olfactory cortical regions. *J*
886 *Comp Neurol* 531: 451-460

887 Isaacson JS, Strowbridge BW (1998) Olfactory reciprocal synapses: dendritic signaling
888 in the CNS. *Neuron* 20: 749-761

889 Klinkenberg I, Sambeth A, Blokland A (2011) Acetylcholine and attention. *Behav Brain*
890 *Res* 221: 430-442

891 Lemasson M, Saghatelian A, Olivo-Marin JC, Lledo PM (2005) Neonatal and adult
892 neurogenesis provide two distinct populations of newborn neurons to the mouse olfactory
893 bulb. *J Neurosci* 25: 6816-6825

894 Lepousez G, Lledo PM (2013) Odor discrimination requires proper olfactory fast
895 oscillations in awake mice. *Neuron* 80: 1010-1024

896 Lin SC, Brown RE, Hussain Shuler MG, Petersen CC, Kepecs A (2015) Optogenetic
897 Dissection of the Basal Forebrain Neuromodulatory Control of Cortical Activation,
898 Plasticity, and Cognition. *J Neurosci* 35: 13896-13903

899 Magavi SS, Mitchell BD, Szentirmai O, Carter BS, Macklis JD (2005) Adult-born and
900 preexisting olfactory granule neurons undergo distinct experience-dependent
901 modifications of their olfactory responses in vivo. *J Neurosci* 25: 10729-10739

902 Malvaut S, Gribaudo S, Hardy D, David LS, Daroles L, Labrecque S, Lebel-Cormier MA,
903 Chaker Z, Cote D, De Koninck P *et al* (2017) CaMKIIalpha Expression Defines Two
904 Functionally Distinct Populations of Granule Cells Involved in Different Types of Odor
905 Behavior. *Curr Biol* 27: 3315-3329 e3316

906 Malvaut S, Saghatelian A (2016) The Role of Adult-Born Neurons in the Constantly
907 Changing Olfactory Bulb Network. *Neural Plast* 2016: 1614329

908 McKenna JT, Yang C, Bellio T, Anderson-Chernishof MB, Gamble MC, Hulverson A,
909 McCoy JG, Winston S, Hodges E, Katsuki F *et al* (2021) Characterization of basal
910 forebrain glutamate neurons suggests a role in control of arousal and avoidance behavior.
911 *Brain Struct Funct* 226: 1755-1778

912 McKenna JT, Yang C, Franciosi S, Winston S, Abarr KK, Rigby MS, Yanagawa Y,
913 McCarley RW, Brown RE (2013) Distribution and intrinsic membrane properties of basal
914 forebrain GABAergic and parvalbumin neurons in the mouse. *J Comp Neurol* 521: 1225-
915 1250

916 Merkle FT, Fuentealba LC, Sanders TA, Magno L, Kessaris N, Alvarez-Buylla A (2014)
917 Adult neural stem cells in distinct microdomains generate previously unknown interneuron
918 types. *Nat Neurosci* 17: 207-214

919 Mirich JM, Williams NC, Berlau DJ, Brunjes PC (2002) Comparative study of aging in the
920 mouse olfactory bulb. *J Comp Neurol* 454: 361-372

921 Murata K, Imai M, Nakanishi S, Watanabe D, Pastan I, Kobayashi K, Nihira T, Mochizuki
922 H, Yamada S, Mori K *et al* (2011) Compensation of depleted neuronal subsets by new
923 neurons in a local area of the adult olfactory bulb. *J Neurosci* 31: 10540-10557

924 Nguyen DP, Lin SC (2014) A frontal cortex event-related potential driven by the basal
925 forebrain. *Elife* 3: e02148

926 Niedworok CJ, Schwarz I, Ledderose J, Giese G, Conzelmann KK, Schwarz MK (2012)
927 Charting monosynaptic connectivity maps by two-color light-sheet fluorescence
928 microscopy. *Cell Rep* 2: 1375-1386

929 Nunes D, Kuner T (2015) Disinhibition of olfactory bulb granule cells accelerates odour
930 discrimination in mice. *Nat Commun* 6: 8950

931 Nunez-Parra A, Cea-Del Rio CA, Huntsman MM, Restrepo D (2020) The Basal Forebrain
932 Modulates Neuronal Response in an Active Olfactory Discrimination Task. *Front Cell*
933 *Neurosci* 14: 141

934 Nunez-Parra A, Maurer RK, Krahe K, Smith RS, Araneda RC (2013) Disruption of
935 centrifugal inhibition to olfactory bulb granule cells impairs olfactory discrimination. *Proc*
936 *Natl Acad Sci U S A* 110: 14777-14782

937 Salcedo E, Tran T, Ly X, Lopez R, Barbica C, Restrepo D, Vijayaraghavan S (2011)
938 Activity-dependent changes in cholinergic innervation of the mouse olfactory bulb. *PLoS*
939 *One* 6: e25441

940 Santiago AC, Shammah-Lagnado SJ (2004) Efferent connections of the nucleus of the
941 lateral olfactory tract in the rat. *J Comp Neurol* 471: 314-332

942 Sanz Diez A, Najac M, De Saint Jan D (2019) Basal forebrain GABAergic innervation of
943 olfactory bulb periglomerular interneurons. *J Physiol* 597: 2547-2563

944 Schoppa NE, Kinzie JM, Sahara Y, Segerson TP, Westbrook GL (1998) Dendrodendritic
945 inhibition in the olfactory bulb is driven by NMDA receptors. *J Neurosci* 18: 6790-6802

946 Shipley MT, Adamek GD (1984) The connections of the mouse olfactory bulb: a study
947 using orthograde and retrograde transport of wheat germ agglutinin conjugated to
948 horseradish peroxidase. *Brain Res Bull* 12: 669-688

949 Valley MT, Henderson LG, Inverso SA, Lledo PM (2013) Adult neurogenesis produces
950 neurons with unique GABAergic synapses in the olfactory bulb. *J Neurosci* 33: 14660-
951 14665

952 Villar PS, Hu R, Araneda RC (2021) Long-Range GABAergic Inhibition Modulates
953 Spatiotemporal Dynamics of the Output Neurons in the Olfactory Bulb. *J Neurosci* 41:
954 3610-3621

955 Yang C, Thankachan S, McCarley RW, Brown RE (2017) The menagerie of the basal
956 forebrain: how many (neural) species are there, what do they look like, how do they
957 behave and who talks to whom? *Curr Opin Neurobiol* 44: 159-166

958 Zaborszky L, Buhl DL, Pobalashingham S, Bjaalie JG, Nadasdy Z (2005) Three-
959 dimensional chemoarchitecture of the basal forebrain: spatially specific association of
960 cholinergic and calcium binding protein-containing neurons. *Neuroscience* 136: 697-713

961 Zaborszky L, Carlsen J, Brashear HR, Heimer L (1986) Cholinergic and GABAergic
962 afferents to the olfactory bulb in the rat with special emphasis on the projection neurons
963 in the nucleus of the horizontal limb of the diagonal band. *J Comp Neurol* 243: 488-509

964 Zhou FW, Hook C, Puche AC (2023) Frequency-dependent centrifugal modulation of the
965 activity of different classes of mitral and tufted cells in olfactory bulb. *J Neurophysiol* 129:
966 1515-1533

967

969 **Figure Legends**

970 **Figure 1. Retrograde labeling of OB-projecting neurons in the HDB/MCPO.**

971 **A:** Schematic of retrograde tracer injections in the OB. CTB = Alexa 555-coupled cholera
972 toxin subunit B. MB = red microbeads. **B:** Coronal section at about bregma from a brain
973 in which microbeads were injected in the left OB. Retrogradely-labeled neurons can be
974 seen in the HDB/MCPO and in the piriform cortex (boxed area on top, enlarged in the
975 middle). Bottom, examples of calretinin-expressing retrogradely-labeled MB+ neurons
976 (arrowheads). **C:** Coronal section at about bregma +0.3 mm from a brain in which Alexa
977 555-coupled CTB was injected in the left OB. This section was immunostained for
978 calretinin (CR, green). Bottom, zoom of the boxed area in the HDB/MCPO. Scale bar 100
979 μm . Captions on the right show the colocalization of CTB and CR in select neurons from
980 the boxed area (arrows). Scale bar 20 μm . **D:** Colocalization of CTB and parvalbumin
981 (PV), CTB and somatostatin (SOM), and CTB and choline acetyl transferase (ChAT) in
982 select neurons (arrows) in the HDB/MCPO. Scale bars 20 μm .

983

984 **Figure 2. CR+ neurons in the HDB/MCPO establish monosynaptic contacts with**
985 **GCs in the OB.**

986 **A:** Experimental timeline for the rabies tracing experiments. **B:** Sagittal section of the OB
987 at P133 showing DsRed+/GFP+ starter cells (yellow). DAPI staining (blue) delimits layers.
988 Note that all cells are located in the granule cell layer (GCL). The mitral cell layer (MCL),
989 the external plexiform layer (EPL), and the glomerular layer (GL) are shown. The boxed
990 area depicts the region in the GCL shown at a higher magnification in panel **C**. **C:** High
991 magnification image of the boxed area in **B**. **D:** Sagittal sections showing GFP+ cells
992 (green) in the MCPO. **E:** Sagittal section showing cells expressing GFP+ cells (green),
993 immunolabeling for CR+ (red), and GFP+/CR+ double-positive cells (yellow) in the
994 HDB/MCPO. **F:** Proportion of HDB/MCPO neurons contacting OB GCs (GFP+ cells) that
995 also express CR.

996

997 **Figure 3. Whole-brain light-sheet imaging of OB-projecting CR+ neurons.**

998 **A:** Schematic drawing showing the experimental procedure for labeling OB-projecting
999 CR+ neurons and whole-brain light-sheet imaging. **B:** Low magnification image of a single
1000 plan (4- μ m-thick) horizontal section of a CR-Cre mouse brain previously injected with
1001 AAVrg in the GCL of the OB. The image shows dense labeling of axonal projections in
1002 the OB and retrograde-labeled neurons in other brain regions. Boxed areas depict regions
1003 for which high magnification images are shown. **C-E:** High magnification images of the
1004 OB (**C**), entorhinal cortex (**D**), and subiculum (**E**) showing retrograde-labeled neurons that
1005 project to the OB. The images were obtained from 500- μ m max projection images, except
1006 for the OB, that show axonal projections in a 4- μ m-thick section. **F:** Low magnifications
1007 image of a single plan (4- μ m-thick) horizontal brain section at the level of the BF and the
1008 piriform cortex of a CR-Cre mouse injected with AAVrg in the GCL of the OB. Boxed areas
1009 depict regions for which high magnification images are shown. **G-I:** High magnification
1010 images of the piriform cortex (**G**), the insular cortex (**H**), and the HDB/MCPO (**I**) showing
1011 retrogradely labeled neurons and axons that project to the OB. The images were obtained
1012 from 500- μ m max projection images. The orientation of sections for B, C and F is shown.
1013 A, P, M, and L indicate anterior, posterior, medial and lateral.

1014

1015 **Figure 4. Conditional expression of ChR2 in CR+ cells in the HDB/MCPO.**

1016 **A:** Schematic representation of the AAV injection protocol to label CR+ cells in the
1017 HDB/MCPO of CR-Cre transgenic mice. **B:** Expression of ChR2-EYFP (green) in CR-
1018 expressing neurons (red) in the HDB/MCPO. **C:** Experimental procedure for
1019 characterizing CR-expressing neurons in the HDB/MCPO. **D:** Photo-evoked whole-cell
1020 responses recorded in the same cell in the current-clamp mode (top) and in the voltage-
1021 clamp mode ($V_h = -75$ mV, bottom). **E:** Membrane voltage responses in the same neuron
1022 as in **D** in response to depolarizing and hyperpolarizing current steps injected through the
1023 patch pipette.

1024

1025 **Figure 5. Optogenetic stimulation of CR+ axons in the OB induce monosynaptic**
1026 **GABAergic responses in GCs.**

1027 **A:** Coronal section of the ipsilateral OB 3 weeks after the conditional viral infection of CR+
1028 neurons in the HDB/MCPO. The right panel is a zoom of the boxed area. Fluorescent
1029 axons (yellow) are concentrated in the granule cell layer (GCL). Arrowheads point to the
1030 few fibers crossing the mitral cell layer (MCL) and entering the external plexiform layer
1031 (EPL). However, none enter the glomerular layer (GL). DAPI staining (blue) delimits the
1032 layers. **B:** Example of a recorded GC filled with biocytin (red). **C:** Synaptic currents
1033 induced by the optogenetic stimulation of ChR2-expressing CR+ axons in the GC shown
1034 in B (top) and average IPSC amplitudes over time for 10 GCs (bottom). Photo-evoked
1035 IPSCs persisted in the presence of NBQX and D-AP5 but were blocked by bicuculline
1036 (BMI). **D:** Passive and active membrane properties of GCs responding and not
1037 responding to the optogenetic stimulation of CR+ axons. No differences in the parameters
1038 were noted.

1039

1040 **Figure 6. Pharmacogenetic inhibition of CR+ neurons in the HDB/MCPO affects**
1041 **odor discrimination/learning in the go/no-go operant conditioning task.**

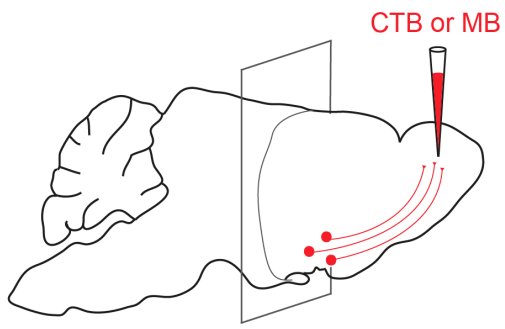
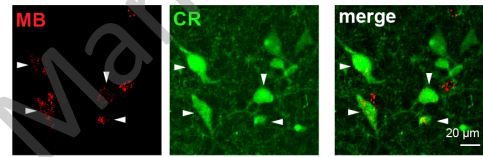
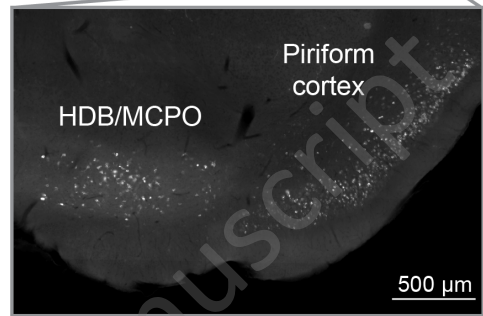
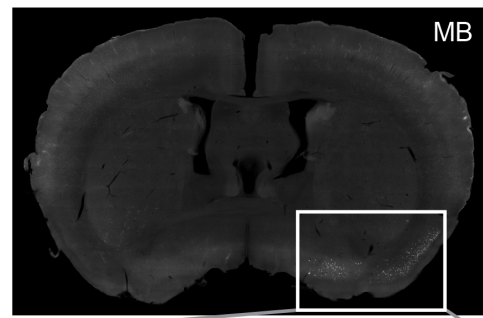
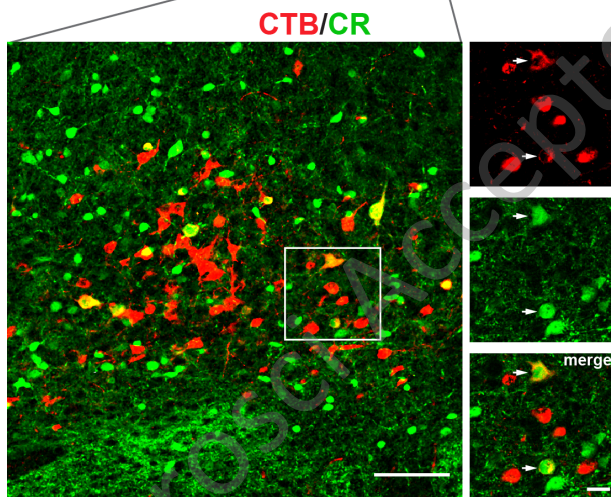
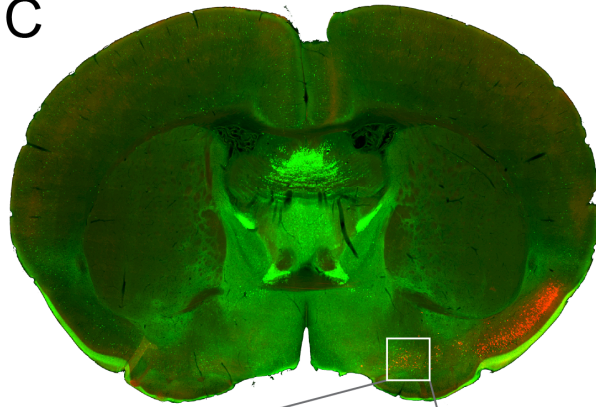
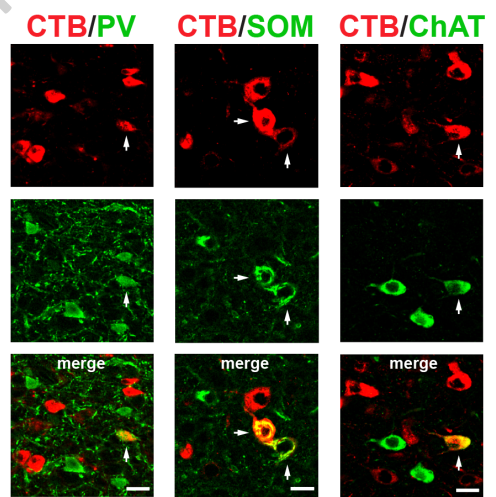
1042 **A:** Schematic representation of a Cre-dependent AAV injection leading to the expression
1043 of either DREADDs or GFP in CR+ cells in the HDB/MCPO of CR-Cre mice. **B:** Schematic
1044 drawing of the go/no-go odor discrimination/learning paradigm. The water-restricted mice
1045 were randomly exposed to reward-associated and non-reward-associated odors (S+ and
1046 S-, respectively), and the percentage of correct responses (hits + correct rejections) was
1047 calculated for every 20 trials. The mice were considered to have successfully
1048 discriminated between the two odors if they reached the 85% criterion of correct
1049 responses. **C:** Low (left) and high (right) magnification images showing that that injection
1050 of Cre-dependent AAV EF1 α -DIO-hM4D(Gi)-mCherry into the HDB/MCPO of CR-Cre
1051 mice results in the selective labeling of CR-expressing mCherry+ cells (red). The sections
1052 were counterstained with DAPI. **D-E:** The mean scores in percentages for each block of
1053 20 trials obtained from the control and DREADDs AAV-injected mice for the go/no-go
1054 odor discrimination/learning task using odor mixtures of different complexity. The odor
1055 pairs used were 0.1% octanal and 0.1% decanal (**D**), and 0.6% (+)-limonene + 0.4% (-)-
1056 limonene and 0.4% (+)-limonene + 0.6% (-)-limonene (**E**). The dashed lines represent the
1057 85% criterion score. * $p < 0.05$ and ** $p < 0.01$ with an unpaired t-test. **F:** Schematic

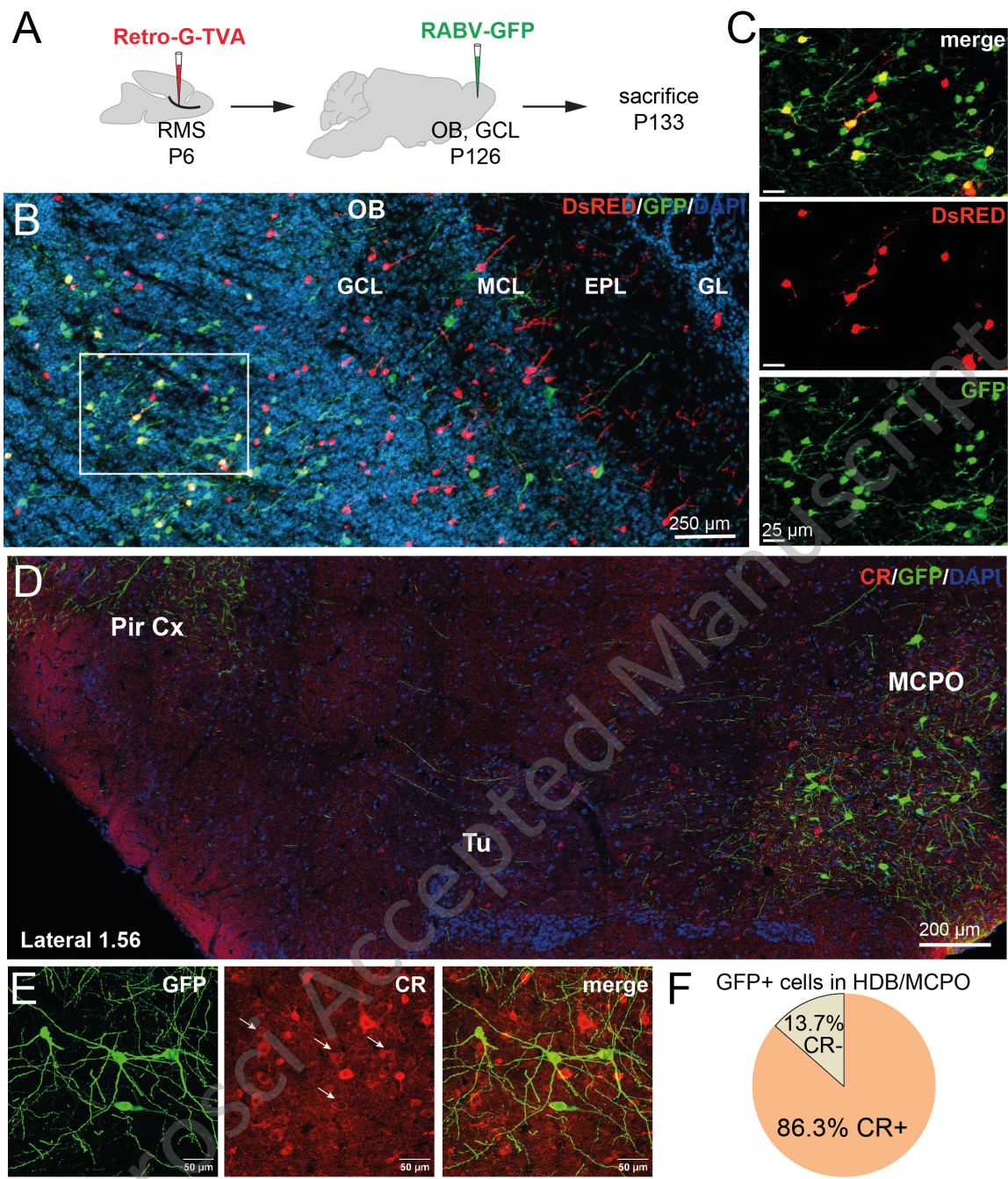
1058 representation of the protocol for AAVrg injections in the OB and fluid cannula installation
1059 above the HDB/MCPO to label and modulate the activity of OB-projecting CR+ cells in
1060 the HDB/MCPO of CR-Cre mice. **G**: The time spent for control (black) and experimental
1061 (grey) mice during the training stage. Note that both groups of mice performed similarly
1062 during the go/no-go training stage. **H**: Low and high (inset) magnification images showing
1063 specific labeling of CR+ cells in the HDB/MCPO by retrograde AAV injections into the OB.
1064 **I**: High magnification confocal images of HDB/MCPO CR+ neurons from the control and
1065 DREADDs-injected mice showing labeling for mCherry (red) and an early immediate
1066 gene, cfos (green). **J**: The percentage of mCherry⁺⁺/cfos⁺ cells in the HDB/MCPO of
1067 control and DREADDs AAVrg-injected mice. *** $p < 0.001$ with unpaired t-test. **K**: The
1068 mean scores of correct responses (in percentages) of control and DREADDs AAVrg-
1069 injected mice subjected to the go/no-go odor discrimination/learning task using odor
1070 mixtures of different complexity. The odor pairs used were 0.1% octanal and 0.1%
1071 decanal (**K**), and 0.6% (+)-carvone + 0.4% (-)-carvone and 0.4% (+)-carvone + 0.6% (-)-
1072 carvone (**L**). * $p < 0.05$ and ** $p < 0.01$ with an unpaired t-test).

1073

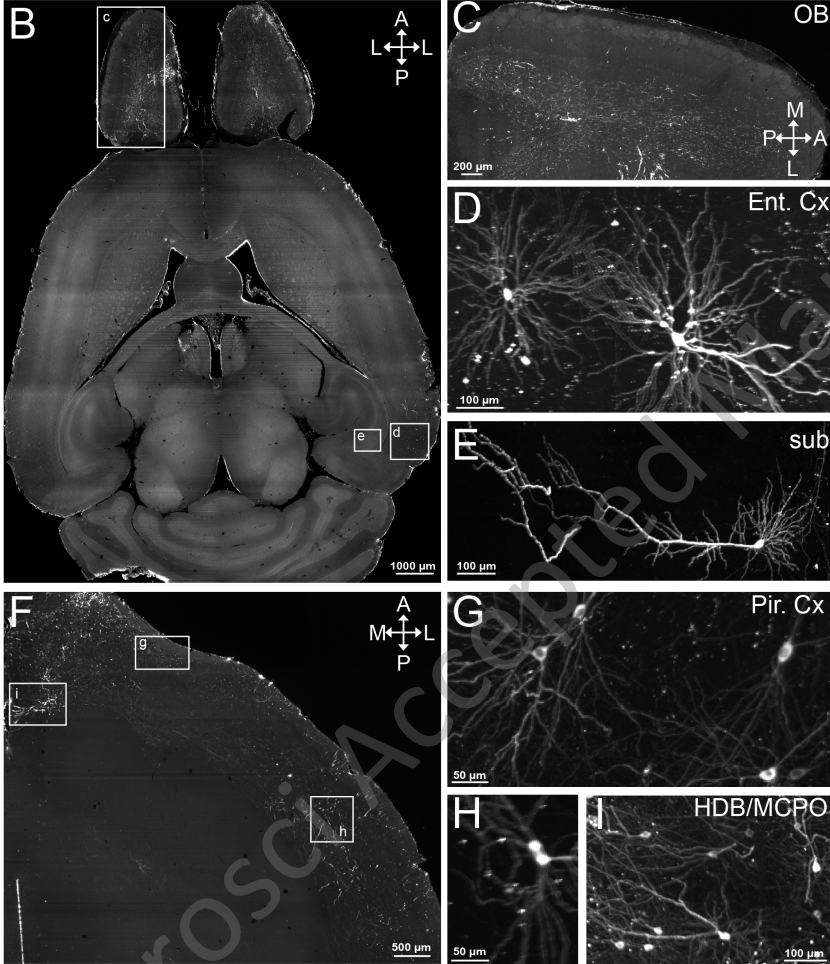
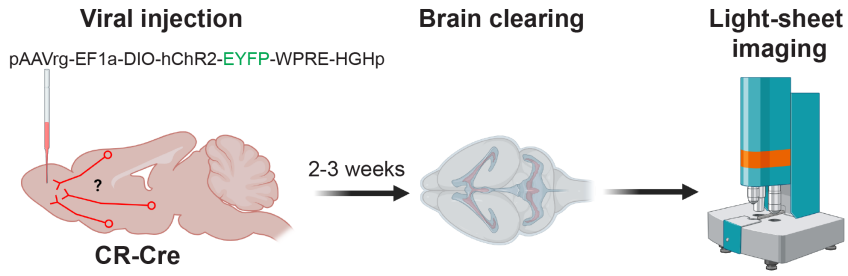
1074 **Figure 7. Pharmacogenetic inhibition of OB-projecting CR+ neurons in the**
1075 **HDB/MCPO do not affect odor discrimination.**

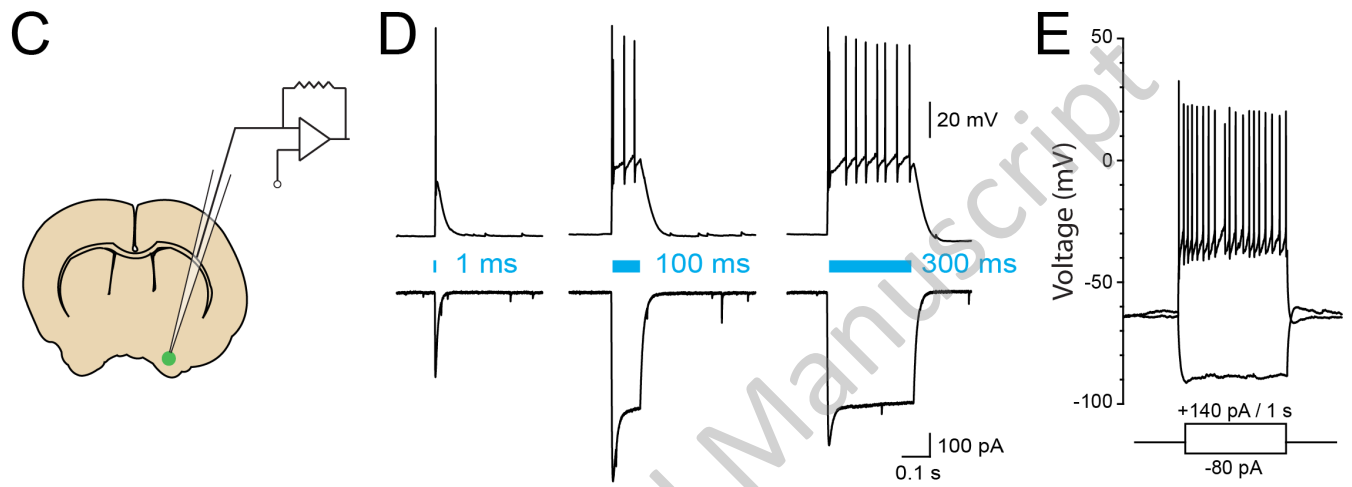
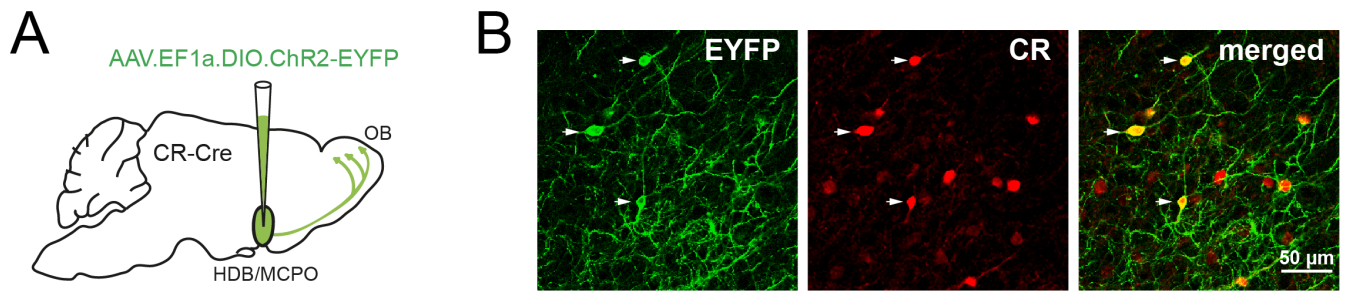
1076 **A**: Schematic representation of the AAVrg injection and fluid cannula installation protocol
1077 to label and modulate the activity of CR+ cells in the HDB/MCPO of CR-Cre mice.
1078 Intracerebral injections of CNO just above the HDB/MCPO were performed 5-10 min
1079 before the test. **B**: Investigation time of control- (black) and DREADDs- (red) injected
1080 mice during habituation and dishabituation sessions. The inset shows the experimental
1081 protocol of the habituation/dishabituation odor discrimination task. Note the similar
1082 performances of both groups of mice and the significant increase in the investigation time
1083 during presentation of the dishabituation odor.

A**B****C****D**



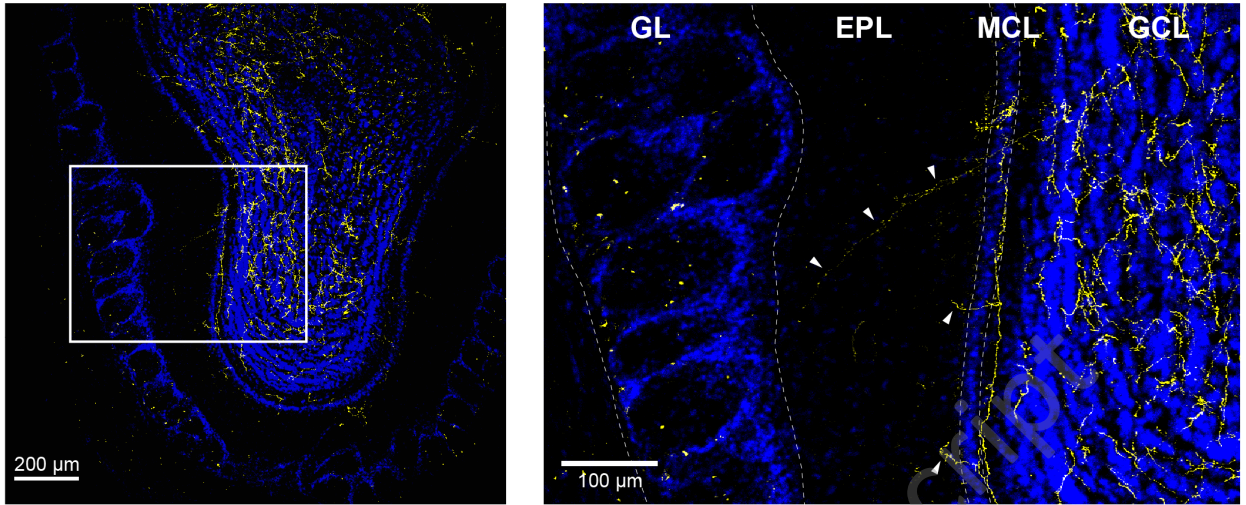
A



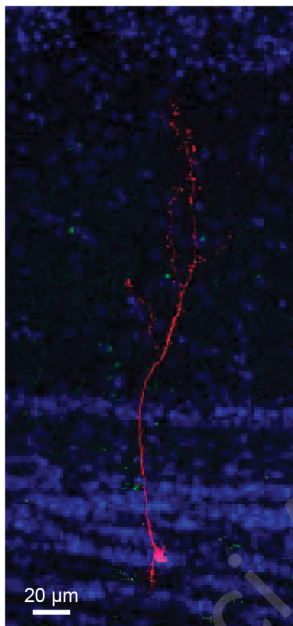


JNeurosci Accepted Manuscript

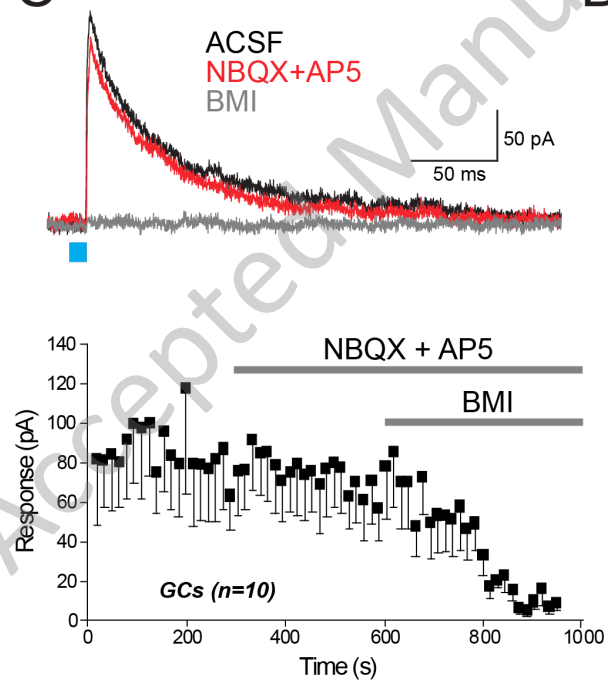
A



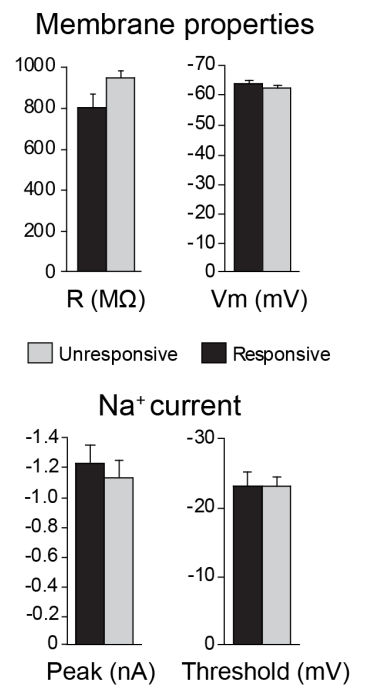
B

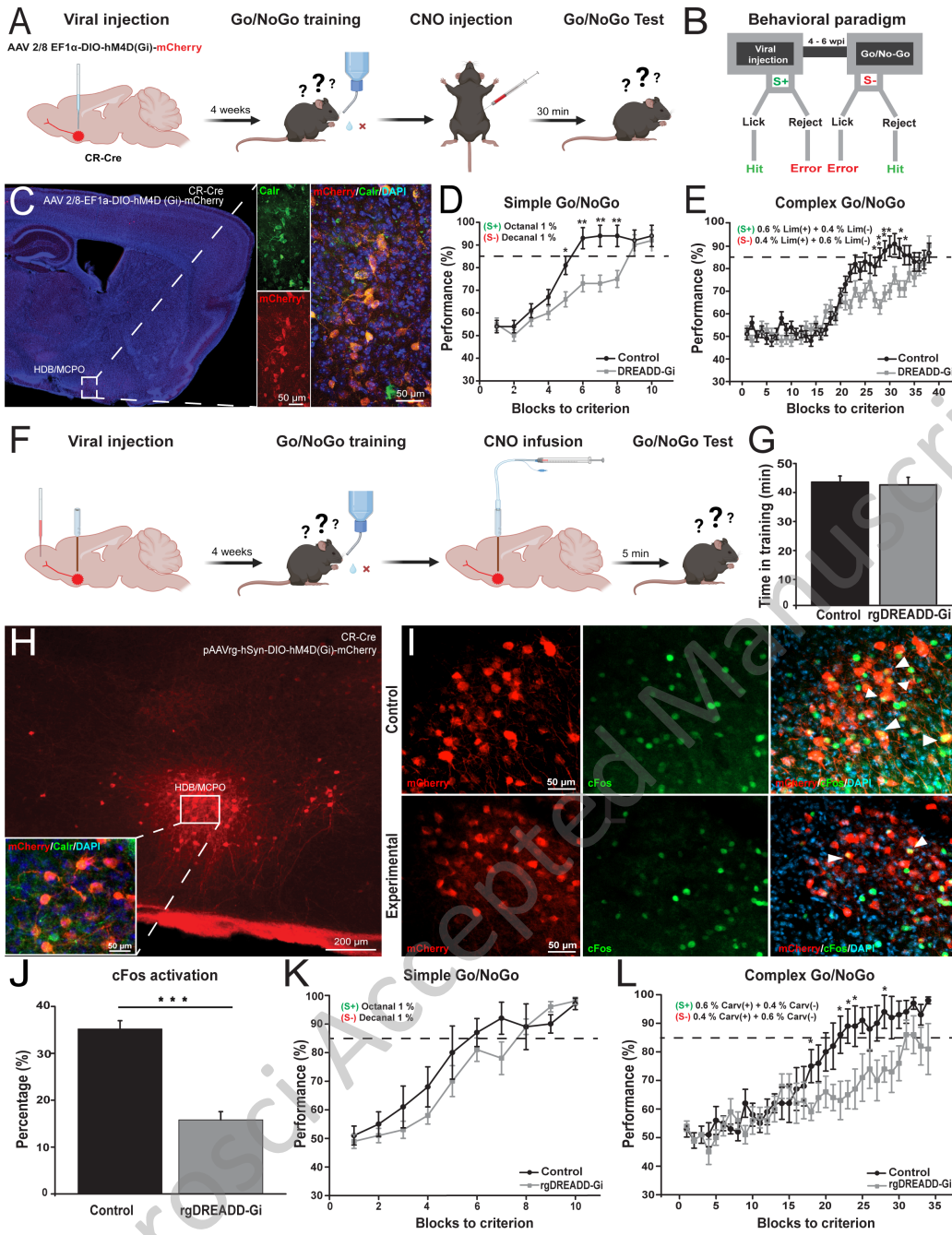


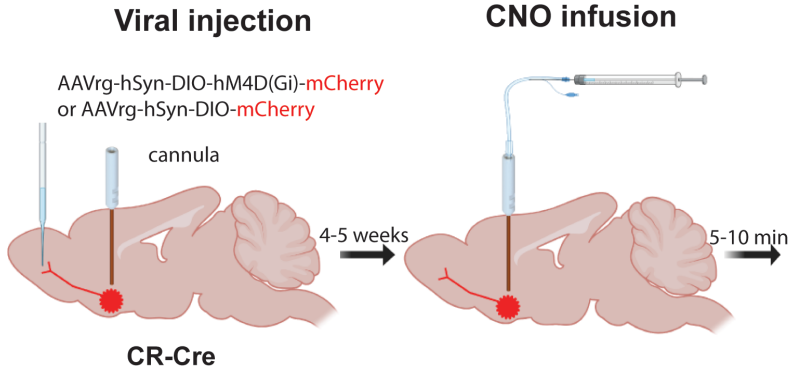
C



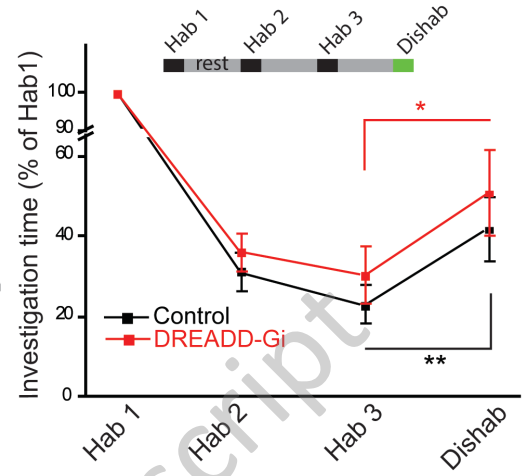
D





A**B**

**Habituation/Dishabituation
odor discrimination task**



JNeurosci Accepted Manuscript